Nucleic Acids Research, 2025, **53**, gkaf271
https://doi.org/10.1093/nar/gkaf271
Nucleic Acid Enzymes

CRISPR RNA binding drives structural ordering that primes Cas7-11 for target cleavage

Calvin P. Lin[1], Harry Li[1], Daniel J. Brogan[2], Tianqi Wang[2], Omar S. Akbari[2], Elizabeth A. Komives[1,*]

[1]Department of Chemistry and Biochemistry, University of California San Diego, La Jolla, CA 92093, United States
[2]School of Biological Sciences, Department of Cell and Developmental Biology, University of California, San Diego, La Jolla, CA92093, United States

[*]To whom correspondence should be addressed. Email: ekomives@ucsd.edu

Abstract

Type III-E CRISPR–Cas effectors, referred to as Cas7-11 or giant Repeat-Associated Mysterious Protein, are single proteins that cleave target RNAs (tgRNAs) without nonspecific collateral cleavage, opening new possibilities for RNA editing. Here, biochemical assays combined with amide hydrogen–deuterium exchange mass spectrometry (HDX–MS) experiments reveal the dynamics of apo Cas7-11. The HDX–MS results suggest a mechanism by which CRISPR RNA (crRNA) stabilizes the folded state of the protein and subsequent tgRNA binding remodels it to the active form. HDX–MS shows that the four Cas7 RNA recognition motif (RRM) folds are well-folded, but insertion sequences, including disordered catalytic loops and β-hairpins of the Cas7.2/Cas7.3 active sites, fold upon binding crRNA leading to stronger interactions at domain–domain interfaces, and folding of the Cas7.1 processing site. TgRNA binding causes conformational changes around the catalytic loops of Cas7.2 and Cas7.3. We show that Cas7-11 cannot independently process the CRISPR array and that binding of partially processed crRNA induces multiple states in Cas7-11 and reduces tgRNA cleavage. The insertion domain interacts most stably with mature crRNA. Finally, we show a crRNA-induced conformational change in one of the tetratricopeptide repeat fused with Cas/HEF1-associated signal transducer (TPR-CHAT) binding sites providing an explanation for why crRNA binding facilitates TPR-CHAT binding.

Graphical abstract

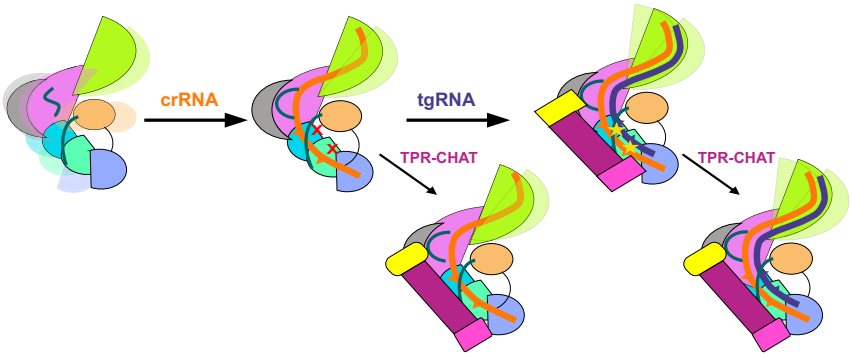

Introduction

CRISPR–Cas systems, composed of various CRISPR–Cas effectors, provide adaptive immunity against invading viruses by interfering with invading nucleic acids [1, 2]. Three types of Cas effectors utilize a programmable CRISPR RNA (crRNA) to recognize and cleave complementary single-stranded target RNA (tgRNA). The multiprotein type III effectors, type III-A (Csm) and type III-B (Cmr), assemble through multiple Cas7 subunits that bind crRNA and cleave single-stranded RNA (ssRNA) [3]. The type VI systems, Cas13a-d, are smaller single-protein effectors with bilobed architecture that target and cleave ssRNA that activates additional nonspecific collateral RNA cleavage [4–6]. While Cas13's off-target collateral cleavage activity has proven useful in developing RNA-sensing diagnostic tools [7, 8], it hinders its application as a gene editing tool due to cell toxicity and organismal lethality [9, 10]. The recently discovered subtype III-E CRISPR–Cas effectors, Cas7-11 or giant Repeat-Associated Mysterious Protein (gRAMP), are RNA targeting single-protein effectors that have potential in RNA manipulation and therapeutic tools [11, 12]. Cas7-11 allows for specific RNA target cleavage without collateral off-target RNA degradation and

Received: September 13, 2024. **Revised:** March 19, 2025. **Editorial Decision:** March 20, 2025. **Accepted:** March 30, 2025

minimal cell toxicity relative to Cas13. Recently, effective trans-splicing of endogenous RNA by Cas7-11 in human cells has been demonstrated [13, 14].

As a descendant of type III-A/B effectors; the type III-E effector, Cas7-11, shares structural and mechanistic elements, particularly within the Cas7 subunits. The evenly spaced Cas7 subunits of type III effectors sport an RNA recognition motif (RRM) βαββαβ fold with a thumb-like β-hairpin that inserts into the crRNA–tgRNA duplex, resulting in flipping of adjacent bases in both strands [15, 16]. A nearby catalytic loop containing a conserved Asp is positioned 3′ to the flipped target base to hydrolyze the scissile phosphate, resulting in a 6-nt target cleavage interval [3, 17].

Cas7-11 is composed of Cas7 domains, (Cas7.1–7.4), a Cas11 domain, the insertion domain (INS), and a carboxy-terminal extension (CTE) domain that are fused together through four linkers (Fig. 1A and D) [18]. Cas7.1 processes the pre-crRNA by cleaving it at position −15 (Fig. 1B) and recognizes and linearizes the 5′-tag of the direct repeat (DR) (Fig. 1C), while Cas7.1–7.4 and the INS recognize the spacer region of the crRNA and the complementary tgRNA [19–21]. The Cas11 domain has been shown to be necessary for positioning the tgRNA for cleavage [18, 20, 21]. Cas7.2 and Cas7.3 have thumb-like β-hairpins responsible for base-flipping in both RNA strands and a conserved Asp residue responsible for tgRNA cleavage, resulting in cleavage in a 6-nt interval 3′ to the flipped 4th and 10th nucleotides [18]. The Cas7.4 domain lacks a β-hairpin and an associated base-flip, and the INS domain is inserted within this domain. The INS domain binds the top of the RNA duplex, although additional functions of the INS remain unknown [18, 21].

Several mechanistic questions arise from differences between Cas7-11 and other type III effectors. *Desulfonema ishimotonii* Cas7-11 (*Di*Cas7-11) is putatively self-sufficient for crRNA processing [11, 18, 19], but *Scalindua brodae* Cas7-11 (*Sb*Cas7-11) does not process its own pre-crRNA [20] and type III-A/B Cas protein complexes process pre-crRNA using ancillary nucleases such as Cas6 or ribonuclease (RNase) E [22, 23].

To gain insight into this new subtype of Cas proteins, we carried out assays to determine whether *Di*Cas7-11 could process CRISPR arrays, and which form of the crRNA was best utilized by *Di*Cas7-11 for tgRNA cleavage. We also performed comprehensive hydrogen–deuterium exchange mass spectrometry (HDX–MS) experiments to characterize the protein dynamics of *Di*Cas7-11 including the apo state (for which no structure is available) and to understand how crRNA and tgRNA binding alter the protein dynamics. We report here that the Cas7 RRM folds are well-structured but a majority of the remaining protein is only weakly folded in the absence of crRNA. Binding of crRNA markedly orders the protein backbone, which strengthens domain–domain interfaces and folds the β-hairpins and catalytic loops within the catalytic sites. Binding of crRNA also reduces the dynamics of the Cas11 domain. The dynamics of the INS varies depending on which crRNA is bound and whether tgRNA is bound. Finally, the HDX–MS data report on regions of *Di*Cas7-11 that could not be resolved in the structure such as those responsible for binding TPR-CHAT (PDB: 8D1V, 7YN9, 7YNA, 7YNB, 7YNC, 7WAH, 8EEX, 7Y9X, 8WMI, and 8WM4) [18, 19, 21, 24–26].

Materials and methods

Protein expression and purification

To generate plasmids for recombinant protein expression, open reading frames of wild-type (WT) *Di*Cas7-11, d*Di*Cas7-11(D429A/D654A), and *Di*Cas7-11ΔINS(979–1293) from plasmids used for mammalian cell culture were subcloned into a modified pET28a vector containing an N-terminal 6×His-SUMO tag as previously described [27].

Plasmids were transformed into Rosetta™2(DE3) pLysS Competent Cells (Novagen). Cells were grown in 1 l LB supplemented with 50 mg/l kanamycin and 34 mg/l chloramphenicol at 37°C until OD_{600} reached ∼1.0. After incubation on ice for 15 min, expression was induced by addition of 0.1 mM isopropyl thiogalactoside (IPTG) followed by continued growth at 18°C for 20 h. Cells were pelleted and resuspended in a lysis buffer containing 50 mM Tris–HCl (pH 8.0), 300 mM NaCl, 10 mM imidazole, 5% glycerol (v/v), and 3 mM β-mercaptoethanol supplemented with Protease Inhibitor Cocktail (Sigma, P2714), 5 mM phenylmethylsulfonylflouride (PMSF), and 2.5 U/ml salt active nuclease (Sigma, SRE0015). Cells were lysed via sonication and clarified by centrifugation at 25 000 × *g* for 30 min. His-tagged protein was bound to 3 ml HisPur™ Ni-NTA Resin (Thermo, 88221) equilibrated with lysis buffer in a glass Econo-Column® (Bio-Rad) by flowing through the clarified lysate. The column was washed with 12 column volume (CV) of wash buffer [50 mM Tris–HCl (pH 8.0), 500 mM NaCl, 30 mM imidazole, 5% glycerol] followed by elution with 7 CV of elution buffer [50 mM Tris–HCl (pH 8.0), 300 mM NaCl, 300 mM imidazole, 5% glycerol]. The 6×His-SUMO tag was removed by dialyzing the eluate overnight at 4°C with ∼0.6 mg of 6×His-tagged Ulp1 (Yeast SUMO Protease) [28] against a dialysis buffer [20 mM HEPES–NaOH (pH 7.5), 250 mM NaCl, 5% glycerol, 1 mM dithiothreitol (DTT)]. Ulp1, the cleaved tag, and additional impurities were removed by flowing the dialyzed sample onto the same Ni-NTA column equilibrated in 20 mM HEPES–NaOH (pH 7.5), 250 mM NaCl, 25 mM imidazole, 5% glycerol, and 1 mM DTT. Cation exchange chromatography was performed on 2 × 1-ml HiTrap Heparin HP Column (Cytiva) with a NaCl gradient from 200–1000 mM NaCl followed by gel filtration chromatography on a HiLoad 16/600 Superdex 200 column equilibrated in 20 mM HEPES–NaOH (pH 7.5), 600 mM NaCl, 5% glycerol (v/v), and 2 mM DTT on an ÄKTA Pure (Cytiva) at 4°C. Fractions were analyzed by sodium dodecyl sulfate–polyacrylamide gel electrophoresis and pure fractions were selected to be concentrated to ∼10 μM and stored in small aliquots at −80°C for future use.

Assays

In vitro cleavage assays

In vitro crRNA processing and tgRNA cleavage assays were performed in 10 μl reactions with the following final concentrations: 40 U Murine RNase Inhibitor (NEB) and 6 mM $MgCl_2$. Other reagents were added as needed at the following concentrations: 500 nM *Di*Cas7-11, 125 nM crRNA/pre-crRNA, 240 nM 6-FAM 5′-labeled tgRNA (ordered from IDT), and 1 U *Escherichia coli* RNase III (Ambion Inc.). The tgRNA was ordered from IDT and is reported in Supplementary Table S1. Reactions were supplemented with

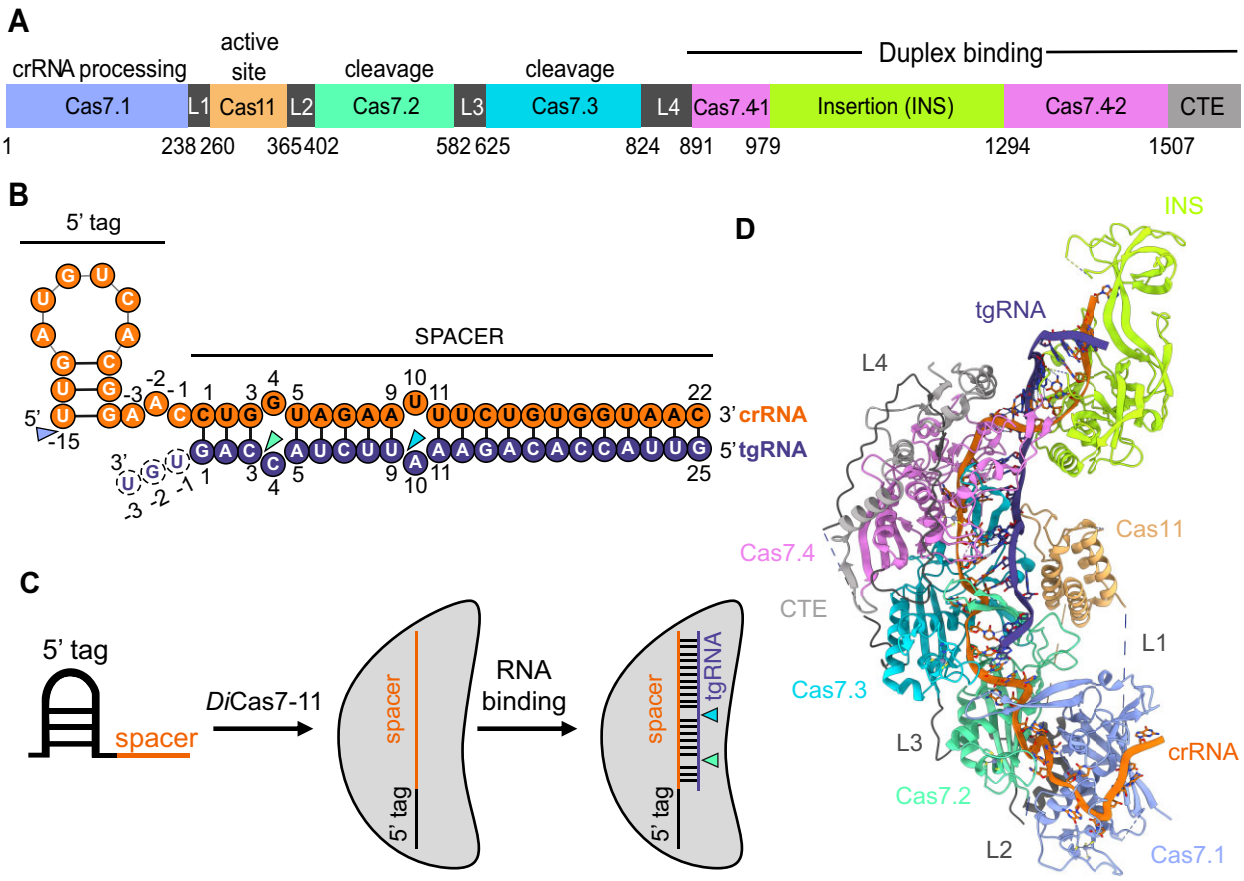

Figure 1. Overview of crRNA, tgRNA, and *Di*Cas7-11 used in HDX–MS experiments. (**A**) Domain organization of *Di*Cas7-11 labeled by their respective functions. The color scheme is used throughout the manuscript to indicate each domain and RNA strand in the structure images. (**B**) Upon *Di*Cas7-11 binding, crRNA is flipped at bases −2, 4, and 10, while tgRNA is flipped at bases 4 and 10. The crRNA processing site and tgRNA cleavage sites are colored by the domain where the respective catalytic residue is found. Target bases −1 to −3, shown with dashed outlines, do not form base pairs. (**C**) Cartoon diagram of the cleavage mechanism. The 5′-tag stem-loop loses secondary structure upon association with *Di*Cas7-11. The crRNA allows for recognition of tgRNA through base pairing, resulting in its subsequent cleavage. (**D**) Structure of *Di*Cas7-11-crRNA-tgRNA (PDB: 7WAH) showing the four Cas7 domains (Cas7.1, Cas7.2, Cas7.3, and Cas7.4), the Cas11 domain, the CTE domain, and the INS connected by linkers.

either 1 µl 10× reaction buffer [200 mM HEPES–NaOH (pH 7.5), 600 mM NaCl] or 1 µl of manufacturer-provided 10× RNase III reaction buffer [100 mM Tris (pH 7.9), 500 mM NaCl, 100 mM $MgCl_2$, 10 mM DTT] when using RNase III. CrRNA processing reactions were incubated for 60 min at 37°C and target cleavage reactions were incubated for 90 min at 37°C. Upon completion, reactions were denatured with 2× RNA dye (NEB, B0363S) at 95°C for 10 min. Samples (10 µl) were then analyzed on a pre-run (200 V for 60 min) 15% tris-borate-EDTA-urea (TBE–urea) PAGE gel (Bio-Rad, 4566055) at 200 V for 35 min. Gels were stained with SYBR Gold (Invitrogen, S11494), incubated for 10 min at room temperature on a shaker, and washed in 1× TBE for 10 min on a shaker before imaging with an ENDURO™ GDS (Labnet).

Electrophoretic mobility shift assays

Ribonucleoprotein complexes (RNPs) were pre-formed by mixing Cas7-11 variants and crRNA at 1:1 final concentration ratio for 20 min before adding to an electrophoretic mobility shift assay (EMSA) master mix [final EMSA contained 40 mM HEPES (pH 7.5), 100 mM NaCl, 5% glycerol, 1 mM DTT, 4 U Murine RNase Inhibitor (NEB), 5 mM ethylenediaminetetraacetic acid, 2.5 µg/ml heparin, and 10 nM 40-nt 6-FAM 5′-labeled tgRNA (IDT)]. Samples were incubated at 37°C for 20 min followed by 20 min at room temperature. Samples were loaded onto a 10% TBE gel and run at 4°C for 36 min at 180 V. Gels were imaged using a G:Box Chemi XX6 (SynGene).

In vitro transcription *for crRNA production*

The *Di*Cas7-11 single array crRNA (IDT) is reported in Supplementary Table S1. All other crRNAs were produced from double-stranded DNA (dsDNA) templates with a T7 promoter as previously described [24]. dsDNA templates were generated from template-less polymerase chain reaction and purified with MinElute PCR Purification Kit (Qiagen, 28004). To convert dsDNA to ssRNA crRNA, *in vitro* transcription was performed using the MEGAScript™ T7 Transcription Kit (Invitrogen, AM1334). SsRNAs were then purified using the MEGAClear™ Transcription Clean-Up Kit (Invitrogen, AM1908).

Hydrogen–deuterium exchange mass spectrometry

*Di*Cas7-11 or the inactive mutant d*Di*Cas7-11 (D429A/D654A) were prepared as described above with

cation exchange followed by gel filtration in H_2O-based HDX buffer composed of 20 mM HEPES (pH 7.5), 150 mM NaCl, 5% glycerol, and 1 mM DTT. $CrRNA_{37}$, $crRNA_{57}$, and 25-nt tgRNA (Supplementary Table S1, IDT) were resuspended in HDX buffer. To form the crRNA–protein complex, protein was incubated with a 2.5 molar excess of crRNA for 1.5 h at 4°C. To form the tgRNA–crRNA–protein complex, 3.75 molar excess tgRNA (to protein), was added to the preformed crRNA–protein complex and incubated for an additional 1 h at 4°C. To prepare the D_2O buffer, the H_2O HDX buffer was subjected to speed vac evaporation and resuspended in an equal volume of D_2O.

HDX–MS experiments were performed using a Waters Synapt G2-Si time-of-flight mass spectrometer equipped with a nanoACQUITY UPLC system with HDX technology and a LEAP PAL liquid handling system. Samples (4 µl) were incubated for 5 min at 25°C and then mixed with 56 µl H_2O buffer, as a control; or D_2O buffer for 30, 60, or 120 s. Controls and timepoints were performed in triplicate. Deuterium exchange was quenched by mixing 50 µl of the protein sample with 60 µl of quench buffer (3 M guanidine hydrochloride, 2.2% formic acid) and incubated for 2 min at 1°C (the pH of the mixed protein-quench solution was measured to be 2.70 at 0°C). The quenched solution (50 µl) was injected onto an in-line pepsin column (immobilized pepsin, Pierce Inc.) at 15°C and resulting peptides were captured on a BEH C18 Vanguard precolumn before separation on a C18 column (Acquity UPLC BEH C18, 1.7 µM, 1.0 × 50 mm, Waters Corporation) using a 7%–85% acetonitrile gradient in 0.1% formic over 7.5 min and directly electrosprayed into the mass spectrometer. The mass spectrometer was set to collect data in the mobility ESI+ mode, with mass acquisition range of 200–2000 (m/z) and scan time 0.4 s. Continuous lock mass correction was accomplished with infusions of leu-enkephalin ($m/z = 556.2771$) every 30 s (mass accuracy of 1 ppm for calibration standard). For peptide identification, the mass spectrometer was set to collect data in mobility MS^E, ESI+ mode instead.

Peptides were identified from triplicate MS^E analyses of 7 µM *Di*Cas7-11 or d*Di*Cas7-11 samples using PLGS 2.5 (Waters Corporation). Peptide masses were identified using a minimum number of 250 ion counts for low-energy peptides and 50 ion counts for their fragment ions. Peptides identified in PLGS were then analyzed in DynamX 3.0 (Waters Corporation) with initial filters as follows: cutoff score of 6.8, minimum products per amino acid of 0.2, maximum MH+ error tolerance of 5 ppm, and retention time standard deviation of 5%. All mass envelopes were manually checked. The deuterium uptake for each peptide was calculated by comparing the centroids of the mass envelopes of the deuterated samples versus the undeuterated controls following previously established methods and deuterium uptake was corrected for back exchange as previously described [29]. Deuterium uptake plots, coverage maps, calculated fractional uptake differences (FUDs), and PDB structures overlayed with HDX data were generated using DECA (github.com/komiveslab/DECA) [30]. The uptake plot *y*-axis maximum is reflective of the total possible amides that can exchange within the peptide and fitted with an exponential curve for ease of viewing using DECA. Community guidelines were followed and are reported in Supplementary Table S2 [31], and the data are publicly available on the Massive data repository (dataset MSV000095504) [31].

Solvent-accessible surface area analysis

Solvent-accessible surface area (SASA) of each residue in *Di*Cas7-11-crRNA was calculated using the areaSAS attribute on a structure of DiCas7-11-crRNA (PDB: 7YN9) in ChimeraX. To obtain SASA values for each peptide observed in HDX–MS, SASA of each residue in a peptide was added together. After removing the crRNA from the structure, the same steps were performed to obtain peptide-level SASA values for apo *Di*Cas7-11. All peptides containing residues that had no electron density in the structure were excluded from the analysis. SASA values were plotted against the back-exchange-corrected deuterium uptake values at 1 min deuterium incubation. ΔSASA and Δdeuterium uptake values of each peptide were used to identify regions of *Di*Cas7-11 that underwent crRNA-induced folding events (Supplementary Table S3), which revealed regions with high degrees of folding as indicated by large deuterium uptake decreases with little or no ΔSASA.

Results

HDX–MS reveals that crRNA binding structures Cas7-11

Cas7-11 appears to have evolved from the linking of four separate Cas7 protein domains [11, 32], so we wondered whether there were interactions between the Cas7 domains or whether they behaved more akin to beads-on-a-string in the apo state. Currently, no apo Cas7-11 structures are available, which could be explained by a flexible architecture of the multidomain Cas7-11. We performed HDX–MS experiments to understand the structure and dynamics of the apo Cas7-11, Cas7-11 bound to crRNA, and Cas7-11 bound to crRNA and tgRNA. TgRNA binding was probed using a catalytically inactive mutant d*Di*Cas7-11-crRNA with and without tgRNA. HDX–MS measures foldedness and solvent accessibility of protein backbones [29, 33]. Following deuterium incubation, reactions were quenched, and proteins were proteolyzed by pepsin for bottom-up peptide identification and HDX analysis. Peptic peptides covered 94.4% of the 1601 amino acid WT protein and 92.1% of the inactive mutant (Supplementary Figs S1 and S2) allowing study of every domain including protein segments not resolved in cryogenic electron microscopy (cryo-EM) structures of WT *Di*Cas7-11-crRNA (PDB: 7YN9) [21] and d*Di*Cas7-11-crRNA-tgRNA (PDB: 7WAH) [18] (Supplementary Fig. S3). The structure of *Di*Cas7-11-crRNA with the crRNA hidden was used to represent the apo state as there is no structure of apo *Di*Cas7-11. The apo protein showed a wide range of deuterium FU at 60 s deuterium incubation time (Fig. 2A). The core of each RRM fold (β1-α1-β2-β3-α2-β4), except the RRM fold of Cas7.1, which forms the convex side of the structure showed low FU in the apo state, suggesting it was well-structured prior to crRNA binding (Fig. 2A) [18]. In contrast, the sequences inserted in the RRM folds, such as the thumb-like β-hairpins and catalytic loops, form a concave crRNA binding surface that exhibits high fractional uptake (FU), indicating high solvent accessibility [18]. The two active sites, the crRNA processing site, the INS domain, and the Cas11 domain all had highly exchanging regions. To compare HDX between different bound states, fractional uptake differences (FUDs) at 60 s deuterium incubation were determined. Upon crRNA addition, marked decreases in exchange (≥−30% FUD) were

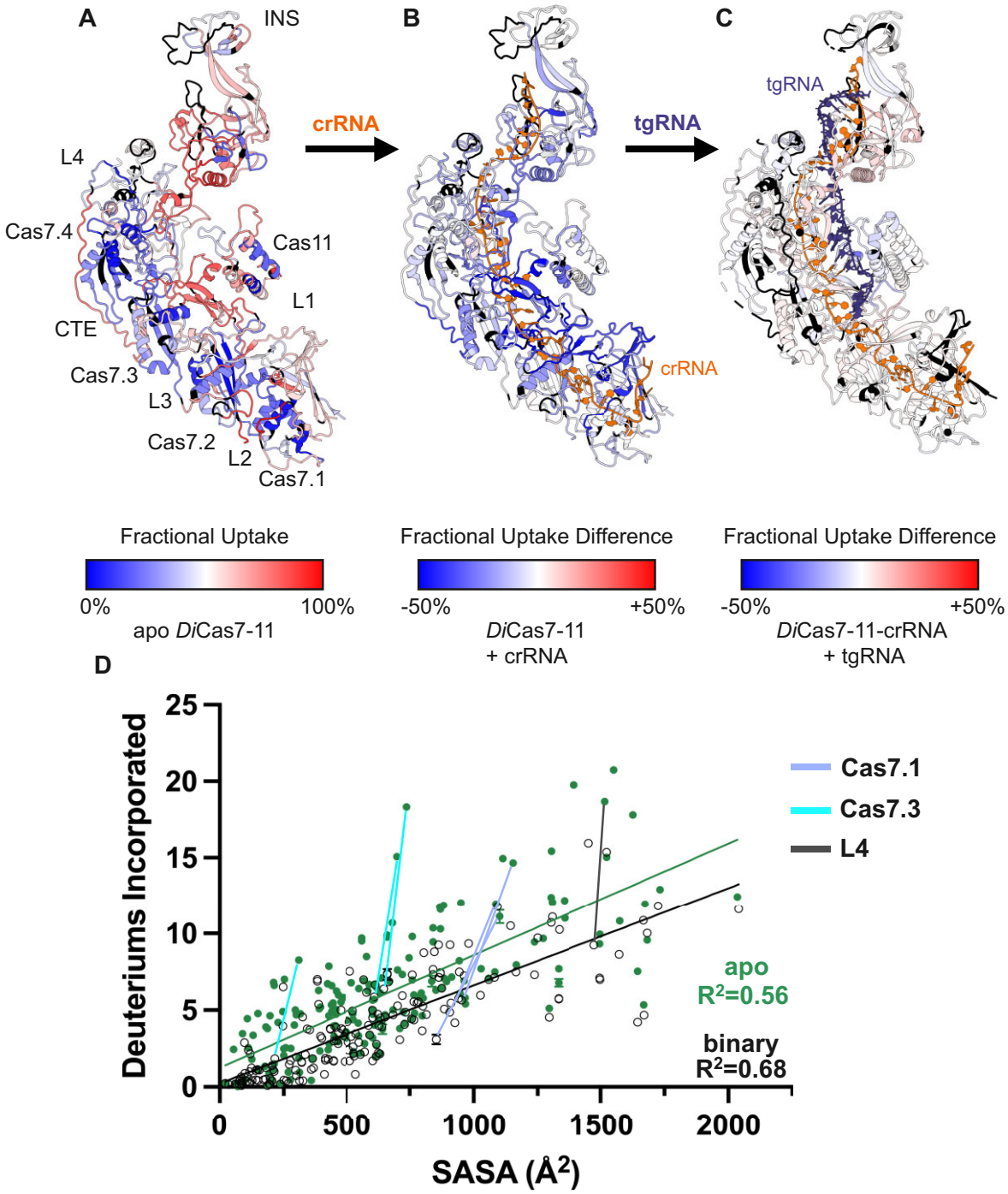

Figure 2. HDX–MS reveals solvent accessibility changes arising from RNA binding. (**A**) FU changes were mapped to a structure of WT crRNA-bound *Di*Cas7-11 (PDB: 7YN9) with crRNA hidden to represent apo *Di*Cas7-11. The structure is colored according to a scale from blue indicating 0% deuterium uptake to red indicating 100% deuterium uptake. All data shown are from 60 s deuterium incubation and are averages of technical triplicates. Regions in black were not covered by peptides from the HDX–MS experiments. (**B**) FUDs, upon crRNA addition to *Di*Cas7-11, were mapped to the same structure as in panel (A) with crRNA (shown in orange). The structure was colored according to FUD on a scale from blue, indicating a 50% reduction in deuterium uptake upon crRNA binding, to red, indicating a 50% increase in deuterium uptake. (**C**) FUD upon tgRNA (shown in dark slate blue) binding to d*Di*Cas7-11-crRNA mapped onto structure of d*Di*Cas7-11-crRNA-tgRNA (PDB: 7WAH). (**D**) The SASA was calculated from the structure of *Di*Cas7-11-crRNA (PDB: 7YN9) and plotted against the HDX–MS deuterium uptake for each peptide in the binary state (*Di*Cas7-11-crRNA) (open black symbols). Then, the crRNA was removed from the structure and the SASA was calculated again and plotted against the HDX–MS deuterium uptake for each peptide from the apo state (solid green symbols). Data are not included for any peptide where electron density was not observed in *Di*Cas7-11-crRNA (PDB: 7YN9). Those peptides showing the largest differences in deuterium uptake but relatively small differences in SASA are indicated by vertical lines connecting the data points of the two states, representative of a high degree of folding.

observed throughout the protein (Fig. 2B). Many highly exchanging regions became very low-exchanging in the crRNA-bound state, suggesting that regions throughout *Di*Cas7-11 folded upon crRNA binding.

To further bolster our conclusion that *Di*Cas7-11 becomes more structured upon crRNA binding, we compared the calculated SASA with the HDX–MS deuterium uptake for the apo versus crRNA-bound *Di*Cas7-11. This approach was previously used to demonstrate that the fifth and sixth ankyrin repeats of IκBα fold on binding to NFκB [34, 35]. Folding upon binding is indicated by a small SASA difference accompanied by a large deuterium uptake difference. SASA calculations were performed on the structure of *Di*Cas7-11-crRNA (PDB: 7YN9). Then, the crRNA was removed from the structure and the SASA was recalculated to represent the apo structure (Fig. 2D). The correlation was higher for the binary state ($R^2 = 0.68$) than for the apo state ($R^2 = 0.56$) indicating that the structure from *Di*Cas7-11-crRNA (PDB: 7YN9) does not represent the apo structure very well. The apo structure had a number of peptides that were highly exchanging and showed much greater reduction of deuterium uptake upon crRNA binding than expected from the SASA difference, indicating that the apo protein is not well-structured in those regions and becomes structured upon binding crRNA (Fig. 2D).

HDX–MS reveals that interdomain interfaces in Cas7-11 are not formed until crRNA binds

Marked decrease in exchange upon crRNA binding was observed at the interfaces between Cas7 domains, suggesting that the structure of apo *Di*Cas7-11 differs significantly from the crRNA-bound structure. Previous cryo-EM structures of the binary (crRNA-bound) and ternary (crRNA and tgRNA-bound) *Di*Cas7-11 (PDB: 7YN9 and 7WAH) suggested that the Cas7 domains were connected by two interfaces—a primary interface composed of the β1-α1 and α2-β4 regions of a Cas7 domain interacting with a β3 strand of a subsequent Cas7 domain, and a second interface in which a thumb-like β-hairpin extends from the previous Cas7 domain to the α1-helix of the next [18].

Our HDX–MS data show that the Cas7.2 β1-α1 (residues 411–420 and residues 411–423), the α2-β4 region (residues 559–570), and the Cas 7.3 β2 strand (residues 718–728) all showed dramatic decreases in deuterium exchange with little change in SASA. The decrease in exchange for the Cas7.3 β3 strand (residues 764–779) was less dramatic (Fig. 3 C and D and Supplementary Table S3). These data suggest that the interdomain interface forms between the Cas7.2 β1-α1 and Cas7.2 α2-β4 interacting with the Cas7.3 β2 strand rather than the β3 strand. In the structure, the Cas7.3 β3 strand is actually further away from the Cas7.2 β1-α1 and α2-β4 regions supporting our interpretation. A similar result was obtained for the Cas7.3 β1-α1 (residues 634–657) and α2-β4 (residues 804–818) interfacing with Cas7.4 β2 (residues 1348–1364) (Supplementary Fig. S4 and Supplementary Table S3).

HDX–MS versus SASA comparison also revealed that the second Cas7 domain interface between the thumb-like β-hairpin and the α1-helix of the subsequent Cas7 domain is formed by crRNA binding. Large decreases in exchange were observed for the Cas7.1 β-hairpin (residues 171–178 and 179–189) and the Cas7.2 α1-helix (residues 431–457) (Fig. 3D and Supplementary Fig. S4D). Similar observations were made for the Cas7.2 β-hairpin (residues 517–532) which interacts with the Cas7.3 α1 (residues 674–687) (Supplementary Fig. S4A) and the Cas7.3 β-hairpin (residues 731–739 and 740–771) which interacts with the Cas7.4 α1-helix (residues 937–949) (Fig. 3B). Altogether, a pattern is observed in which the secondary interface is formed between the already folded α1-helix and the unfolded thumb-like β-hairpins that fold upon interaction with the α1-helix when crRNA binds.

The L3 and L4 linkers and the CTE are also thought to contribute to stabilizing Cas7 interdomain interactions. HDX results show that the L3 linker (residues 581–606, 607–619, and 620–630) is surprisingly protected from exchange in both the apo and crRNA-bound states (Supplementary Table S3). This linker connects Cas7.2 to Cas7.3 through stabilizing hydrophobic interactions with Cas7.2 α2. The Cas7.2–Cas7.1 interface may also be stabilized by an L3 interaction with the Cas7.1 α2-helix [18]. In contrast, the L4 linker (residues 810–838) shows one of the largest decreases in exchange upon crRNA binding (Fig. 2D). A long loop in the CTE that extends from the Cas7.4 β4 strand (residues 1503–1530) interacts with α2 from Cas7.3 (residues 783–800). Both of these regions showed large decreases in exchange upon crRNA binding but no change in SASA (Supplementary Table S3). Altogether, the HDX–MS results show that L3 stabilizes the domain interfaces in the apo state whereas the interfaces involving L4 and the CTE form upon crRNA binding. The results are most consistent with a model in which the Cas7 domains in apo *Di*Cas7-11 behave like beads-on-a-string, and only form a unified structure upon crRNA binding (Fig. 2B and C).

crRNA binding induces structuring of the pre-crRNA processing site

Prior to RNP complex formation between Cas effectors and their evolved crRNA, crRNAs must be processed following CRISPR array transcription [32]. *Di*Cas7-11, is somewhat unique, as it is able to bind and process the 35-nt 5′ DR of pre-crRNA to a 15-nt 5′-tag and by cleaving off an additional 20-nt stem-loop [11]. The Cas7.1 pre-crRNA processing site showed pronounced decreases in deuterium uptake ranging from −30% to −47.6% FUD (Fig. 4A and B) with varying amounts of SASA changes upon crRNA binding.

Exchange decreases were localized to the region surrounding the scissile phosphate, including the β strands of the RRM folds. Residues 33–39 and 99–106 near the active site showed decreases in SASA and FU, suggesting that the decreased exchange is attributable to crRNA interaction. The β1 strand of Cas7.1 (residues 39–60), containing the pre-crRNA processing active site residue H43 [18], underwent a marked decrease in deuterium uptake (−40.1% FUD) (Fig. 4B, black arrow) and showed little SASA change. This region is adjacent to the β2-β-hairpin (residues 147–173), which also markedly decreased in exchange with little SASA change (Fig. 4B). These data strongly suggest coupled folding of these regions upon crRNA binding. Residues 190–203 which form an antiparallel β-sheet with residues 147–173 had a FUD change of −18.3% upon crRNA binding with no SASA change showing that this peptide undergoes some degree of structuring. Altogether, HDX–MS suggests that a large portion of the domain comprising the crRNA processing site folds upon binding crRNA, revealing the crRNA's role in active site formation. By comparing the results from residues 147–170 and 147–173, it is possible to conclude that the nonoverlapping residues,

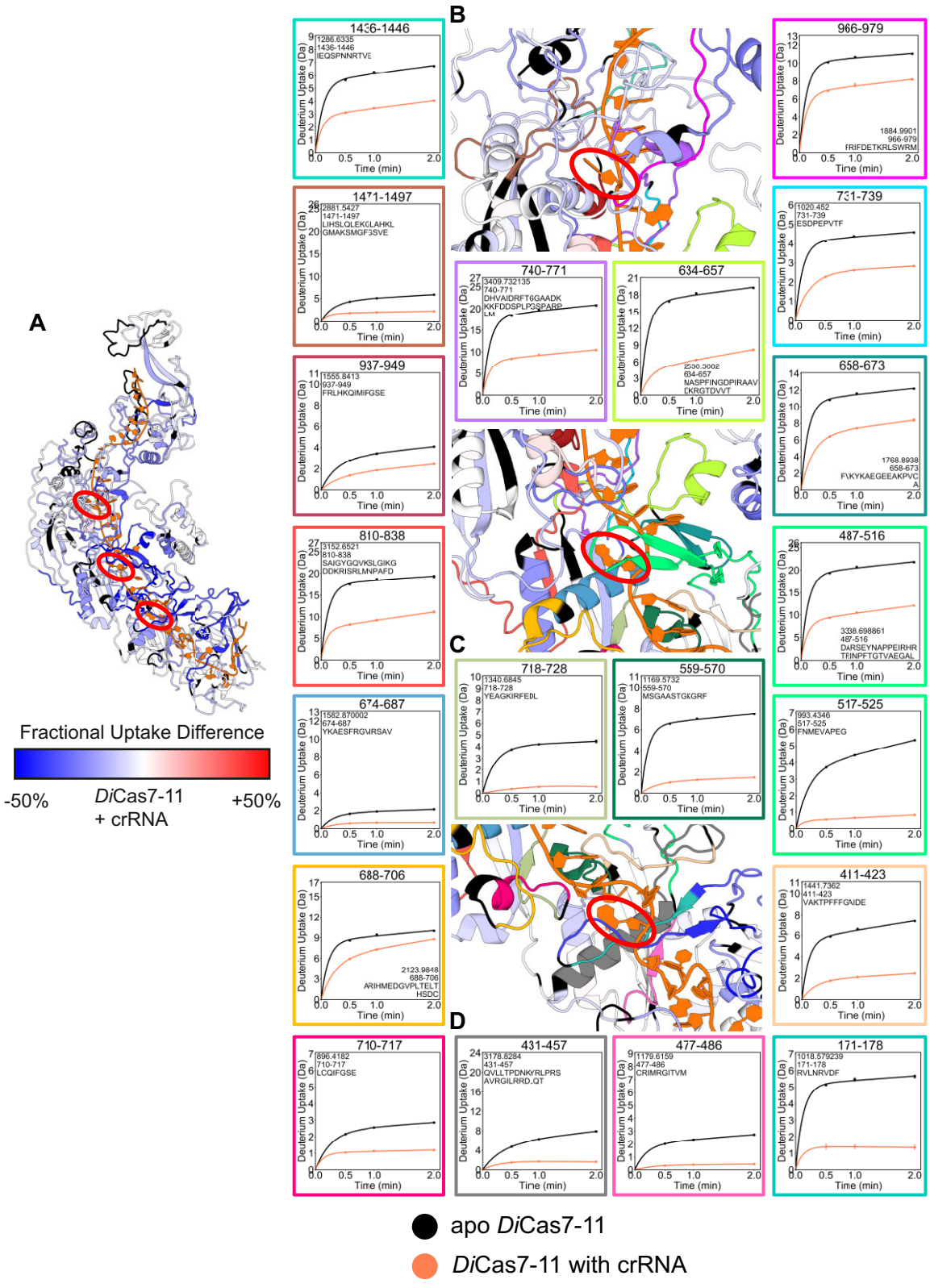

Figure 3. HDX–MS reveals that crRNA binding induces protection of domain interfaces and catalytic sites. (**A**) FUD upon crRNA binding at 60 s deuterium incubation was mapped to *Di*Cas7-11-crRNA structure (PDB: 7YN9). Flipped crRNA bases are circled in red. (**B**) Zoomed inset at the Cas7.3/Cas7.4 interface, colored by FUD and corresponding uptake plots, where Cas7.3-mediated target cleavage occurs. Data are shown as mean values ± standard error of the mean of three technical replicates with the *y*-axis maximum corresponding to the maximum possible deuterium uptake. The flipped crRNA base is circled in red. The selected uptake plots show significant uptake decreases from highly solvent exposed states in the apo state suggesting folding upon binding and initially solvent protected regions in the apo state, suggesting pre-folded regions that form new protein or RNA interactions. (**C**) Zoomed inset at the Cas7.2/Cas7.3 interface where Cas7.2-mediated target cleavage occurs. (**D**) Zoomed inset at the Cas7.1/Cas7.2 interface.

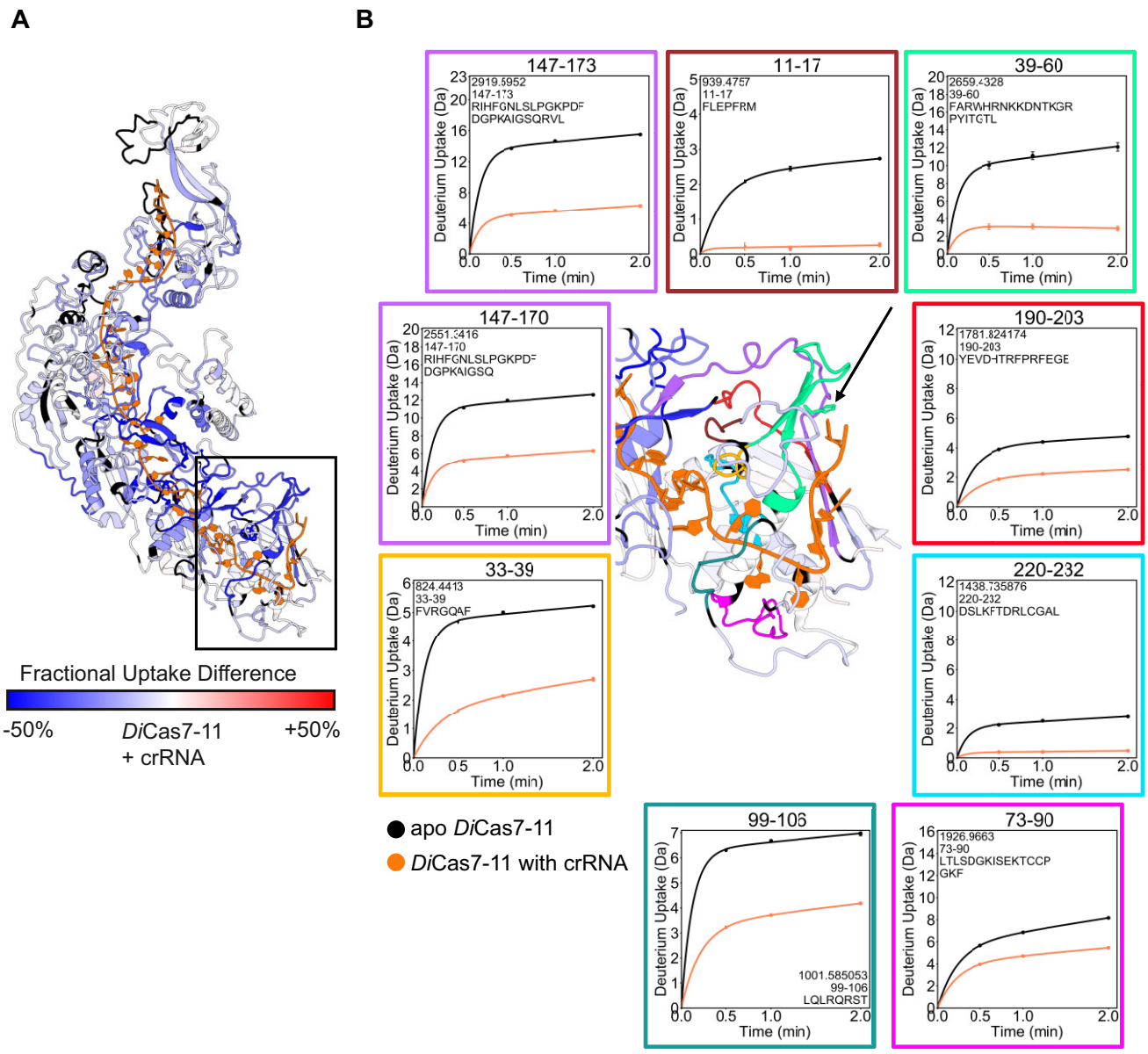

Figure 4. HDX–MS reveals crRNA-binding effects in the processing site of *Di*Cas7-11. (**A**) FUD upon crRNA binding mapped to *Di*Cas7-11-crRNA structure (PDB: 7YN9) with inset box around Cas7.1. (**B**) Zoomed-in inset of Cas7.1 domain colored by corresponding HDX uptake plots. Other regions are colored according to FUD, while regions not detected by MS are shown in black. Black arrow points to H43, WT *Di*Cas7-11's catalytic residue for pre-crRNA processing. Black circles represent apo *Di*Cas7-11 while orange circles represent *Di*Cas7-11 bound to crRNA.

171–173 of the β-hairpin undergo complete protection upon crRNA binding, likely due to newly formed intra-protein or flipped base interactions [18, 19, 21, 25].

crRNA structurally rearranges regions near base-flipping centers and catalytic loops

The thumb-like β-hairpins of the Cas7.1–7.3 domains perform two functions—they support the domain–domain interactions, and they interact with crRNA and tgRNA nucleotides between the two flipped bases to prevent them from base-pairing [3, 15, 18, 21]. Our data suggest that the Cas7.1–7.3 β-hairpins fold upon crRNA binding (Fig. 3A–D). While the β-hairpin of Cas7.1 interacts with the Cas7.2 α1-helix and the crRNA flipped base, it is not involved in cleavage because Cas7-11 has a shorter tgRNA than other type III effectors [3, 18, 36] and no conserved catalytic Asp in the Cas7.1 catalytic loop [16, 18, 37]. Residues I504/V682 of Cas7.3 and M953/K1489, previously shown to "sandwich" the flipped 4th and 10th crRNA bases in the ternary complex structure (PDB: 7WAH) [18] were contained in peptides covering residues 487–516, 674–687, 1471–1497, and 937–965 that showed decreases in deuterium uptake upon crRNA binding (Fig. 3B and C and Supplementary Fig. S4A and C).

The catalytic loops of Cas7.2 (residues 411–423) and Cas7.3 (residues 634–657) which are equivalent to the β1-α1 motifs of the second interface (Fig. 3C and D), showed marked decreases in exchange upon crRNA binding and little SASA indicating structuring upon crRNA binding (Fig. 2D and Supplementary Table S3). Catalytic residues in these two loops are responsible for cleaving the phosphodiester bond 3′ to the corresponding flipped base. However, part of the Cas7.2 catalytic loop (residues 424–430), containing the

active site residue, D429, showed no change (Supplementary Fig. S4B), suggesting that structuring only occurs immediately N-terminal to the catalytic residue. Smaller peptides comprising the Cas7.3 catalytic loop residues 634–646 and 647–657 (which include the Cas7.3 active site residue, D654) also showed strong protection (FUDs of −64.1% and −40.5%) indicating that the entire Cas7.3 catalytic loop undergoes structuring (Supplementary Fig. S4A).

tgRNA binding induces localized changes near the active site residues responsible for target positioning for cleavage

The d*Di*Cas7-11-crRNA binary complex and the d*Di*Cas7-11-crRNA-tgRNA ternary complex were also studied by HDX–MS. TgRNA binding resulted in additional changes in deuterium uptake localized to both active sites comprised of the thumb-like β-hairpins and catalytic loops. The deuterium uptake differences were more subtle than those induced by crRNA binding, likely, because the crRNA-bound state was already folded. Structures of the ternary complex (PDB: 8D1V, 7WAH) [19, 20] reveal that the tgRNA bases adjacent to the Cas7.2 and Cas7.3 thumb-like β-hairpins flip toward the catalytic loops, positioning the scissile phosphate closer to the catalytic residues D429 and D654 (Fig. 5A and B). However, previous studies showed no structural change in the Cas7.2 and Cas7.3 domains of *Di*Cas7-11-crRNA (PDB: 7YN9, 8D1V) [19, 21] upon tgRNA binding (PDB: 7YNA, 7WAH) [21, 25]. Similar results were obtained when the crRNA-bound and crRNA and tgRNA-bound type III-A/B complexes were compared [15, 16]. The β-hairpin of Cas7.3 was covered by two peptides. The longer peptide (residues 740–771) showed a decrease in exchange, whereas the shorter peptide (residues 751–763) showed an increase (Fig. 5A). Similar results were obtained for Cas7.2 where residues 487–516 showed a decrease and overlapping residues 487–510 showed an increase upon tgRNA binding (Fig. 5B). Since these two peptides partially overlap, these results imply that the region of the longer peptide that is not included in the shorter peptide decreases even more than what is measured in the longer peptide. This pattern of increased exchange within a region of decreased exchange indicates a dynamic conformational change upon tgRNA binding likely coupled to the tgRNA base flipping and opening of the RNA duplex.

The Cas7.2 and Cas7.3 catalytic loops showed decreased exchange upon tgRNA binding indicating that tgRNA binding further structures the catalytic loops. Residues 424–430 of Cas7.2, which contains the inactivated catalytic residue D429A, showed decreased exchange upon tgRNA binding (Fig. 5B). A peptide adjacent to the Cas7.2 catalytic loop (residues 411–423) showed increased deuterium uptake upon tgRNA binding (Fig. 5A). Residues 634–657, which cover the inactivated catalytic residues D654A of Cas7.3, showed decreased exchange that could be localized to residues 647–657 because another peptide, residues 634–646 showed no difference upon tgRNA binding (Fig. 5A). Again, the adjacent increased and decreased exchange suggests a conformational rearrangement that may be involved in positioning the catalytic loop and the active site residue.

Further analysis of the mass spectra corresponding to peptides from the Cas7.3 catalytic loop revealed additional conformational flexibility induced by tgRNA binding. A bimodal mass envelope was observed for residues 634–657 (Fig. 5C) upon tgRNA binding, indicating induction of an equilibrium between two conformations, one of which is exchanging substantially more deuterium than the other [38–40].

We interpret this to mean that tgRNA binding induces a slow opening of residues 634–657, relative to the deuterium incubation timescale. This behavior was also seen in residues 411–423, although to a lesser extent (Fig. 5D). While our HDX–MS analysis was visualized using a structure of the catalytically inactivated ternary complex, d*Di*Cas7-11-crRNA-tgRNA (PDB: 7WAH), we note that the structure of the WT ternary complex DiCas7-11-crRNA-tgRNA (PDB: 8D1V) is nearly identical. This is probably because *Di*Cas7-11-crRNA was incubated with tgRNA for only 10 min prior to flash freezing and cleavage occurs on a slow timescale [19]. Thus, our HDX–MS data also describe the conformations of the active binary and ternary complexes prior to tgRNA cleavage. Collectively, these uptake decreases and conformational changes within the catalytic loops and β-hairpins likely reveal structural rearrangements that enable effective target cleavage.

crRNA binding primes Cas11 domain for target cleavage

Biochemical evidence from Cas11 domain deletions as well as single point mutations indicates that Cas11 is necessary for tgRNA cleavage [18, 20, 41, 42]. It is thought that Cas11 properly orients the tgRNA [18, 21, 41] while the β-hairpins flip the crRNA and tgRNA bases and keep them away from each other [3, 18, 21, 43]. Structural studies have shown that several Cas11 side chains interact with the tgRNA phosphate backbone and the 3rd and 9th bases near the cleavage sites [18, 20, 41, 42]. Cas11 residues 274–284 and 285–298 showed −16.8% and −26.7% FUD, respectively (Fig. 6A). Residues 329–335 showed very low uptake values and slower deuterium uptake kinetics, and crRNA binding reduced the deuterium uptake to 0 (Fig. 6A). Cas11 did not exhibit significant change in SASA upon crRNA binding, as it does not contact the crRNA in the *Di*Cas7-11-crRNA structure. However, HDX–MS data showed >50% of the domain undergoes FUD decreases upon crRNA binding indicating that Cas11 is somehow more dynamic and less structured prior to crRNA binding.

tgRNA binding further reduced exchange in residues of the Cas11 domain (Fig. 6B). Residues 274–284 showed −16.8% FUD upon crRNA binding (Fig. 6A), and further reduction was observed upon tgRNA binding (FUD of −7.6%) (Fig. 6B). Residues C-terminal to this region, 285–298 and 299–328 showed marked decreases in exchange upon crRNA binding but little change upon tgRNA binding (Fig. 6B and Supplementary Fig. S5). HDX data suggest that most of the structural ordering in Cas11 occurs prior to tgRNA binding with smaller, localized changes occurring upon tgRNA engagement.

HDX–MS reveals structural flexibility of the INS domain in response to different RNAs

Independent studies have shown that deletion of the INS domain (*Di*Cas7-11Δ979–1293) [18–21] does not significantly affect RNA cleavage or knockdown, although one study showed an enhanced cleavage rate upon INS deletion [21]. Moreover, the structure of the INS domain varies significantly across orthologs [44] and is even required for target

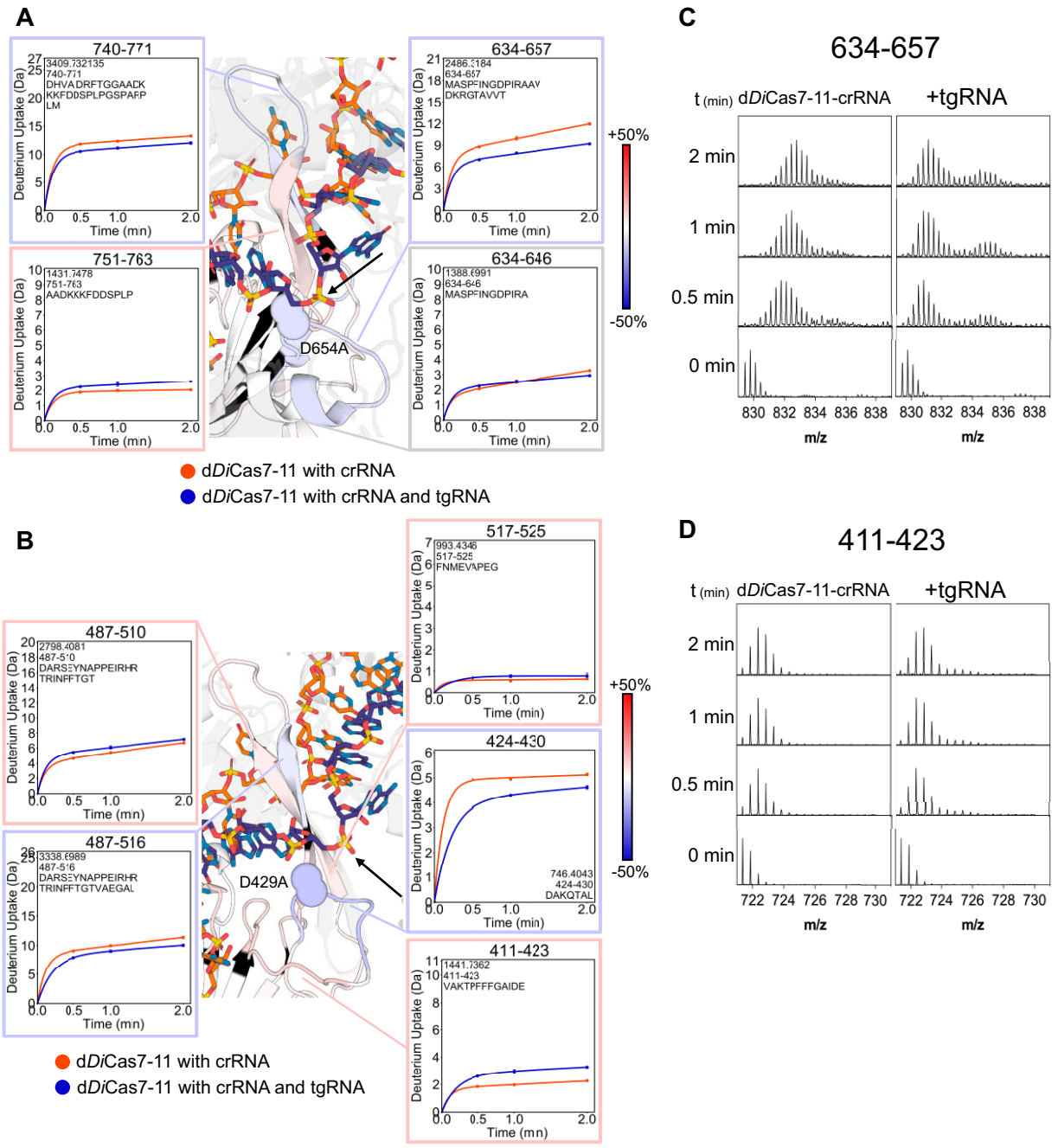

Figure 5. tgRNA-induced changes in d*Di*Cas7-11 active sites. Zoomed-inset showing thumb-like β-hairpins and catalytic loops of (**A**) Cas7.3 and (**B**) Cas7.2 domains in a d*Di*Cas7-11-crRNA-tgRNA structure (PDB: 7WAH). FUD of tgRNA binding was mapped to the structure with regions not showing significant FUD in gray. Orange–red symbols in the deuterium uptake plots represent d*Di*Cas7-11-crRNA while blue symbols represent d*Di*Cas7-11-crRNA-tgRNA. Black arrows on the structure point to tgRNA scissile phosphates adjacent to flipped bases. Mass spectra showing a bimodal mass envelope for the catalytic loops of the (**C**) Cas7.3 and (**D**) Cas7.2 domains upon tgRNA binding, suggesting two interconverting conformations with significantly different deuterium uptake.

cleavage in *Sb*Cas7-11 [42]. We also observed that deletion of the INS had no effect on catalytic activity (Fig. 7A). EMSAs of WT *Di*Cas7-11-crRNA and *Di*Cas7-11(ΔINS)-crRNA showed that binding to tgRNA was also unaffected (Fig. 7B and C). While an uptake plot of residues 1025–1037 (Fig. 7D) indicated a decrease in exchange upon crRNA binding, further analysis of the mass spectra showed that this decrease resulted from the appearance of bimodal mass envelopes (Fig. 7E), indicating two interconverting conformational states. HDX–MS analysis of the INS domain showed that bimodal mass spectral envelopes were observed across most of the INS domain (Supplementary Fig. S6) and mapped onto the *Di*Cas7-11-crRNA structure (PDB: 7YN9) (Fig. 7F). We also note that centroids of the higher m/z state in all analyzed peptides had the same m/z as the centroids observed for the apo state. These data can best be interpreted to indicate that the INS may be binding and unbinding to the 3′ end of the crRNA.

Subsequent tgRNA binding to d*Di*Cas7-11-crRNA yielded a slight increase in deuterium uptake across the INS domain (Fig. 2C) as represented by the peptide corresponding

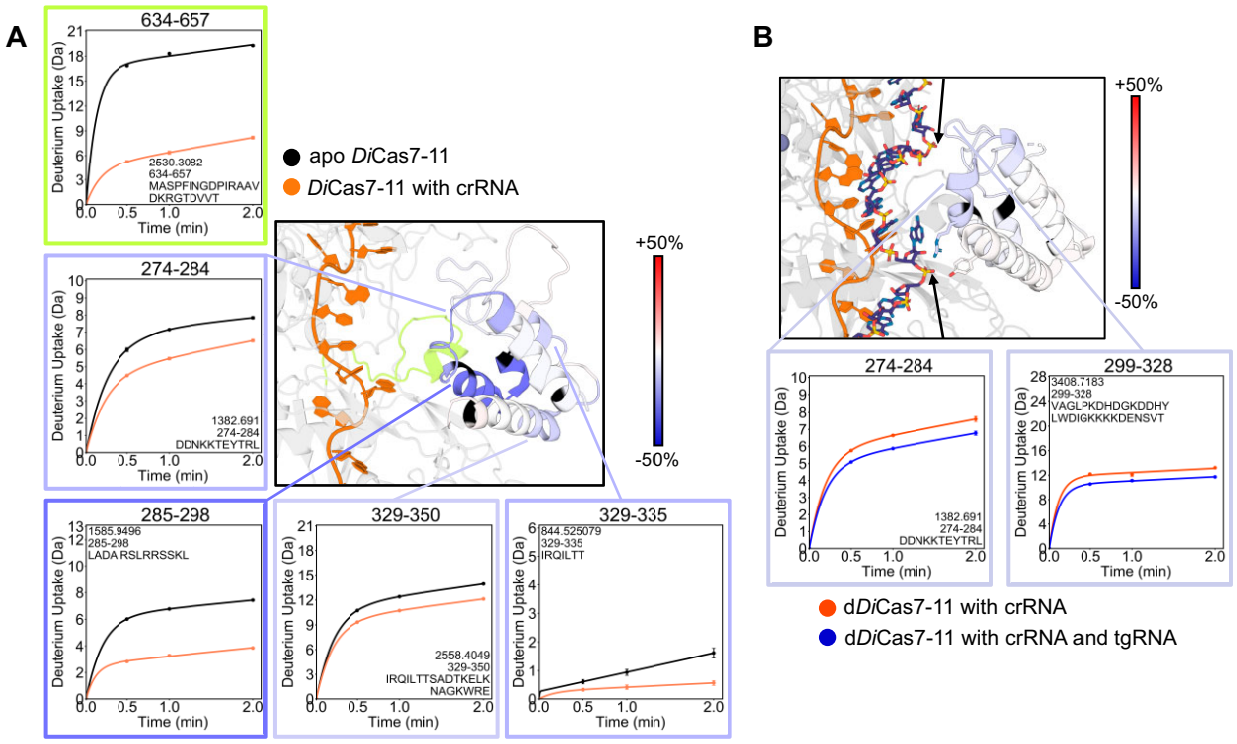

Figure 6. The Cas11 domain showed decreased exchange upon crRNA-binding but little additional change upon tgRNA-binding. (**A**) FUD of crRNA-binding to WT *Di*Cas7-11 mapped to PDB: 7YN9. Cas11 is colored by FUD with associated HDX uptake plots, while the rest of the protein is shown in gray. Lines from uptake plots point to their respective location on the structure. The region corresponding to residues 634–657 that appears to interface with Cas11 in *Di*Cas7-11-crRNA is shown in lime. (**B**) FUD of tgRNA-binding to d*Di*Cas7-11-crRNA mapped to PDB: 7WAH. Residues previously shown to be essential for cleavage activity in *Sb*Cas7-11 are shown as sticks. Scissile phosphates are marked by black arrows.

to residues 1025–1037 (Fig. 7G). d*Di*Cas7-11-crRNA showed similar bimodal distributions for the INS domain as compared with the WT *Di*Cas7-11-crRNA. Subsequent tgRNA binding led to a decrease in the proportion of the less solvent exposed state (lower m/z) (Fig. 7H). This effect was consistently observed across all mass spectra with bimodal distributions observed in the crRNA binding experiment (Supplementary Fig. S7) and the regions of the INS that show this behavior are mapped onto the ternary complex structure PDB: 7WAH in Fig. 7I. The more solvent exposed state had a centroid with similar m/z to the centroid observed in the apo WT state (Fig. 7E and Supplementary Figs S6 and S7). Taken together, we interpret these results to mean that crRNA binding gives rise to an equilibrium between two states within the INS domain and that tgRNA binding shifts the equilibrium toward a conformation that interacts less well with the 3′ end of the crRNA and the 5′ end of the tgRNA.

DiCas7-11 processes pre-crRNA while host nucleases mature functional crRNA

It is not clear from previous work whether *Di*Cas7-11 can only perform crRNR processing or whether it can also perform maturation [11, 18, 27]. To assess this, we compared the *Di*Cas7-11 processing activity of a single array-like transcript containing the DR on both 5′ and 3′ ends of a 22-nt spacer with the more commonly used 3′-less single array transcript with a DR only on the 5′ end of a 22-nt spacer [11, 18, 19, 21, 24] (Fig. 8A–C). While *Di*Cas7-11 processes a pre-crRNA with only a 5′ DR to the mature 37-nt crRNA, henceforth referred to as $crRNA_{37}$, *Di*Cas7-11 processes the single array-like transcript into a partially processed crRNA, (referred to as $crRNA_{57}$), that contains the mature 15-nt 5′-tag 5′ to the spacer and an additional 3′ 20-nt stem-loop (Fig. 8C). *In vitro* cleavage assays with *Di*Cas7-11-$crRNA_{57}$ revealed reduced target cleavage at the Cas7.3 active site (Fig. 8D). Whereas tgRNA binding to *Di*Cas7-11-$crRNA_{37}$ yielded only the highest band, which we presume to be the fully formed, catalytically active ternary complex (Fig. 8E), *Di*Cas7-11-$crRNA_{57}$ binding to tgRNA yielded multiple species with a lower population of the fully formed complex. INS deletion mutants yielded a similar pattern (Fig. 8E).

Because our results indicated that *Di*Cas7-11 can process crRNA arrays but cannot perform maturation steps, and because RNase III was shown to process the crRNR into crRNA of other Cas effectors [45], we assessed the products from mixing pre-crRNA with RNase III with or without added *Di*Cas7-11. Our results show that RNase III is capable of cleaving both DRs in the DR-spacer-DR single array with products corresponding to $crRNA_{57}$ and $crRNA_{37}$, although the DR-spacer-DR single array cleavage product had a slightly higher size than $crRNA_{37}$ (Supplementary Fig. S8).

HDX–MS allowed for comparison of solvent accessibility of the WT *Di*Cas7-11 complex with the mature $crRNA_{37}$ versus the WT *Di*Cas7-11 complex with the partially mature $crRNA_{57}$. The additional 3′ 20-nt stem-loop is expected to be positioned after the last resolvable nucleotide at the 3′ region near the INS domain (PDB: 7YN9, 7WAH, 8D1V [19]). Higher solvent accessibility throughout the INS domain was observed in the $crRNA_{57}$ binary complex represented by residues 1025–1037 (Fig. 8F and G). Mass spectra (Fig. 8H and Supplementary Fig. S6) revealed bimodal

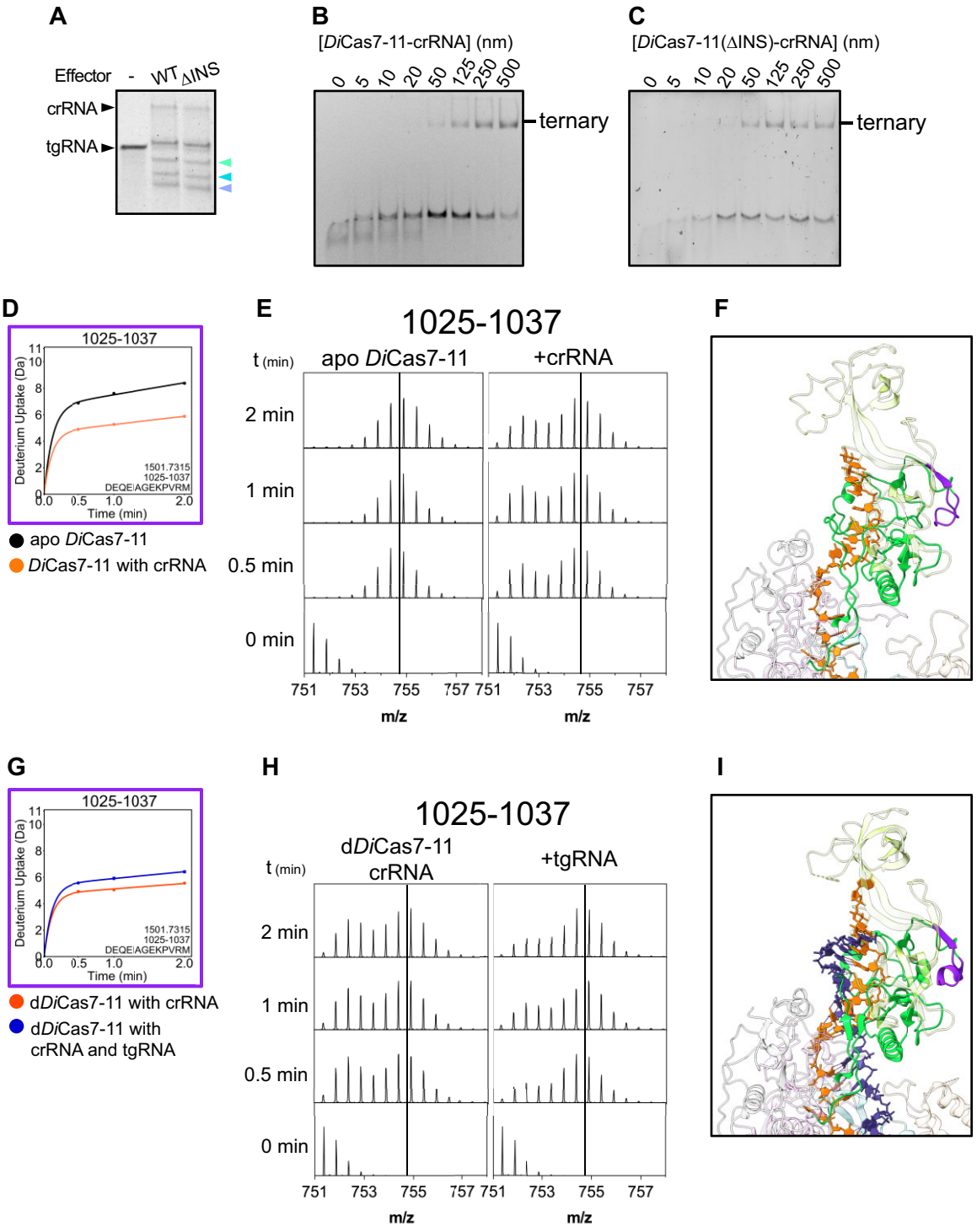

Figure 7. The INS domain is conformationally heterogeneous. (**A**) *In vitro* cleavage assay shows that INS deletion does not affect tgRNA cleavage. Target products were marked by their respective Cas7.2 and Cas7.3 domain colors. The lowest cleavage product was from Cas7.1 processing. (**B**, **C**) EMSAs of WT *Di*Cas7-11-crRNA and ΔINS *Di*Cas7-11-crRNA show similar tgRNA binding. (**D**) Uptake plot of residues 1025–1037 showing effects of crRNA binding. (**E**) Raw mass spectra of residues 1025–1037 showing formation of a bimodal mass envelope upon crRNA binding, indicating interconversion between two different conformations. Black lines through the *y*-axis show that the centroids have equal *m*/*z* values, suggesting that the associated conformations have a similar environment across states. (**F**) Structure of INS domain (PDB: 7YN9) with residues 1025–1037 in purple and other residues exhibiting bimodal mass envelopes upon crRNA binding in green. The rest of the structure is transparent for ease of viewing. (**G**) Uptake plot of residues 1025–1037 showing effects of tgRNA binding. (**H**) Raw mass spectra of residues 1025–1037 showing an increase in the more exchanging conformation upon tgRNA binding, suggesting a more open INS domain. (**I**) Structure of INS domain (PDB: 7WAH) with residues 1025–1037 in purple and other residues exhibiting bimodal mass envelopes upon crRNA binding in green.

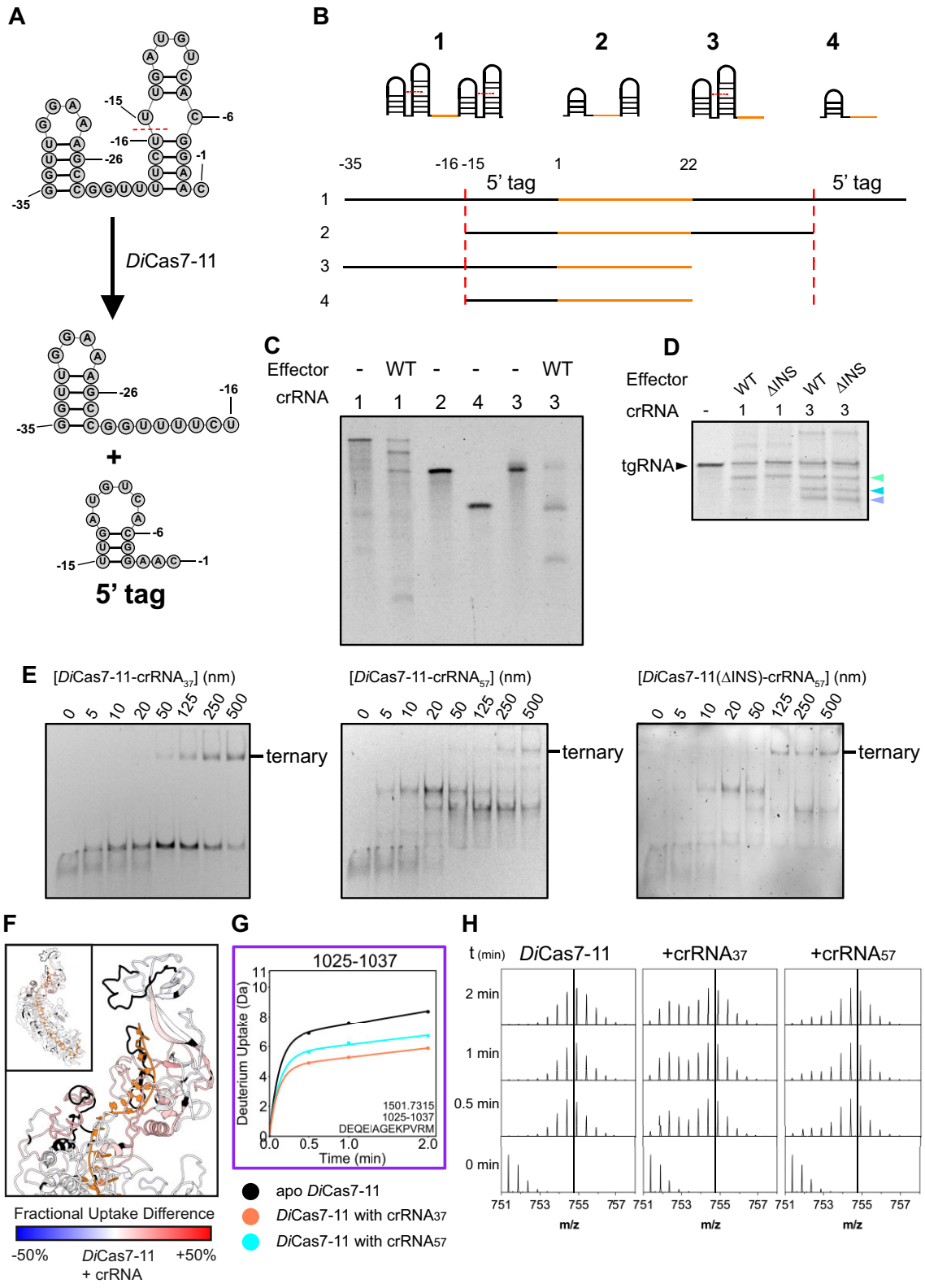

Figure 8. *In vitro Di*Cas7-11 pre-crRNA processing leads to a product that reduces tgRNA cleavage. (**A**) 35-nt *Di*Cas7-11 DR shown with secondary structure. Cas7.1 cleaves the DR at red dashed line, forming two products—a 15-nt 5′-tag recognized by the Cas7.1 domain, and a 20-nt strand with stem-loop structure. (**B**) Pre-crRNAs, 1 (single array) and 3 (5′ DR-spacer), and crRNAs, 2 (crRNA$_{37}$) and 4 (crRNA$_{57}$), used for *in vitro* cleavage and binding assays are shown with Cas7.1 cleavage sites marked by red dashed lines. 3 and 4 are commonly used in processing assays. (**C**) *Di*Cas7-11 processing of various crRNAs. (**D**) Processing and target cleavage assays reveal the crRNA 2 (crRNA$_{57}$) leads to lowered target cleavage. (**E**) tgRNA in the presence of increasing *Di*Cas7-11-crRNA$_{37}$, *Di*Cas7-11-crRNA$_{57}$, or *Di*Cas7-11(ΔINS)-crRNA$_{57}$ reveal that crRNA$_{57}$ leads to lowered amount of properly formed RNP. (**F**) Uptake plot of peptide 1025–1037. (**G**) FUD between *Di*Cas7-11-crRNA$_{57}$ and *Di*Cas7-11-crRNA$_{37}$ shows *Di*Cas7-11-crRNA$_{57}$ has higher solvent accessibility near 5′ end of the tgRNA, where a stem-loop may be present. (**H**) Raw mass spectra of uptake plot showing varied distributions upon binding different crRNAs, suggesting a more open INS domain in *Di*Cas7-11-crRNA$_{57}$ relative to *Di*Cas7-11-crRNA$_{37}$.

deuterium envelopes with less of the lower *m/z* envelope, reminiscent of those induced by tgRNA in the same peptides in the *Di*Cas7-11-crRNA$_{37}$ sample. The *in vitro* processing and cleavage assays not only showed that *Di*Cas7-11 cannot process pre-crRNA itself but also that its processing product, crRNA$_{57}$, leads to reduced tgRNA cleavage. Taken together, binding assays and HDX–MS suggest that the crRNA$_{57}$ does not form an active ternary complex as effectively as crRNA$_{37}$ and results in a more open *Di*Cas7-11 INS domain.

crRNA induces structural changes in TPR-CHAT interaction motifs

While our study focuses on the RNA-guided nuclease activity of *Di*Cas7-11, the data also shed light on how the RNA-guided Craspase complex forms. The protease TPR-CHAT, or Csx29, is part of the Cas7-11 CRISPR locus, and binds Cas7-11-crRNA to form the Craspase complex that is involved in the protease-mediated immune response [20, 21, 24, 46, 47]. Several structural studies have characterized two primary TPR-CHAT binding interfaces on *Di*Cas7-11 with residues 367–401 in L2 and 1313–1341 in the Cas7.4–2 domain, hereafter referred to as Craspase Interface 1 and Craspase Interface 2 (CI1 and CI2), respectively. These motifs lack electron density (PDB: 7YN9, 8D1V, 8WM4, 7WAH) until TPR-CHAT binds, suggesting TPR-CHAT binding may induce structure in these regions (PDB: 8WMC, 7Y9X, 7YND) [18, 19, 21, 25, 26]. Because these regions are not observed in structures prior to TPR-CHAT binding, HDX–MS can yield important information about the structures of the binding regions prior to TPR-CHAT binding (Fig. 9). HDX–MS showed that CI1 is highly exchanging in both the apo and crRNA-bound *Di*Cas7-11 (Fig. 9B). *Di*Cas7-11 CI2 residues 1313–1341 were covered by two peptides—residues 1308–1322 which showed a decrease in deuterium uptake upon crRNA binding, and residues 1325–1346 which showed an increase (Fig. 9B).

The concomitant increase and decrease in exchange suggest that this region undergoes a conformational change upon crRNA binding. A previous study showed that the N-terminal domain (residues 1–65) of TPR-CHAT—TPR-CHAT^{NTD}—is sufficient for binding *Di*Cas7-11 and forms a primarily hydrophobic interface with CI2 [26]. Follow-up studies showed that *Di*Cas7-11Δ1317–1336 did not interact with TPR-CHAT^{NTD} [26]. However, it is important to note that the same deletion does not prevent interaction with full-length TPR-CHAT indicating that other regions of TPR-CHAT besides the NTD may contribute to the interaction [21, 25, 26]. Our HDX–MS results show that crRNA binding induces a conformational change in CI2 whereas tgRNA binding to d*Di*Cas7-11 did not appear to elicit significant changes in either interface. These results indicate that crRNA binding remodels the CI2 interaction site in *Di*Cas7-11 required for TPR-CHAT recruitment (Supplementary Fig. S9).

Discussion

HDX–MS analysis of apo *Di*Cas7-11 provided critical information regarding how structure determines function in this interesting Cas protein family. A lack of structural information on the apo state underscores the importance of using biophysical methods along with structural biology [48]. The Cas7 domains are RRM folds that have sequence inserts that bind the crRNA, induce base flipping, and catalyze target cleavage. Structures with crRNA bound show the four Cas7 domains form an overall crescent shape with the crRNA bound in the inner concave surface [18, 19, 21, 49]. HDX–MS revealed that the convex side of the crescent shaped *Di*Cas7-11, formed by the canonical β1-α1-β2-β3-α2-β4 segments of the RRM folds in each Cas7 domain had low deuterium exchange. Similarly, other RRM fold proteins used for RNA recognition have structured RRM folds prior to RNA binding [50–52]. In contrast, the concave surface corresponding to the additional inserted sequences were highly exchanging and appear to fold upon binding to the crRNA. In addition, the interdomain contacts seem mostly absent in the apo protein except for the L3 interactions with Cas7.2 and Cas7.3. CrRNA binding caused very large decreases in exchange that could only be explained by structuring of the Cas7 insertion sequences and interdomain interactions.

The literature is unclear as to whether *Di*Cas7-11 can process the CRISPR array transcript into a mature crRNA *in vitro* [10]. Studies co-expressing *Di*Cas7-11 or *Sb*Cas7-11 with their respective CRISPR arrays in *E. coli* have shown that crRNAs are processed to their mature sizes, with 15- and 18-nt 5′-tags, respectively, followed by ∼20-nt spacers [11, 12]. Using a single array transcript, we showed that *Di*Cas7-11 leaves an additional 20-nt 3′ hairpin (as seen in crRNA$_{57}$). This lack of maturation was not known because most studies use a pre-crRNA with no 3′ DR and consequently no 3′ hairpin upon processing (crRNA$_{37}$). The observation that *Di*Cas7-11 is unable to process pre-crRNA makes sense because its ortholog *Sb*Cas7-11 is also unable to process pre-crRNA [12, 41, 42, 49, 53] and type III-A/B complexes require other host nucleases for crRNA maturation [3]. These results strongly suggest that for all Cas7-11 proteins an ancillary nuclease such as RNase III, from the host organism will be needed to cleave the DR 3′ to the spacer.

The INS domains of type III-E Cas effectors are highly variable, and their function is unknown. The INS domains in *Di*Cas7-11 are only partly resolvable (PDB: 7Y9X, 8GS2) [21, 25] or not at all visible (PDB: 8D1V, 8WMC, 8WMI, 8WM4, 8EEX) [19, 24, 26] in the available structures. No density for the INS domain of *Sb*Cas7-11 (*Sb*gRAMP) has been observed in any structural studies [20, 41, 42, 49, 53] suggesting that *Sb*Cas7-11 has a more flexible INS than *Di*Cas7-11. Our HDX data are consistent with the INS domain being highly flexible. Functionally, the INS domain of *Di*Cas7-11 can be deleted and the catalytic activity for tgRNA does not change [18, 19]. The 3′ 20-nt hairpin in crRNA$_{57}$ would be positioned near the INS, so we probed whether the INS could sense the difference between the partially processed crRNA and the fully processed crRNA$_{37}$. HDX–MS revealed that the entire INS domain was interconverting between two different conformations upon crRNA binding, one that was more protected and one that was significantly less protected from exchange. More of the protected conformation was observed in *Di*Cas7-11-crRNA$_{37}$ when compared with *Di*Cas7-11-crRNA$_{57}$. The predominance of the less protected conformation suggests that the INS domain does not interact with the crRNA$_{57}$ as well as with the crRNA$_{37}$.

Our HDX–MS data reveal how *Di*Cas7-11 is structured for catalytic function. The individual RRM domains are not even fully interacting prior to crRNA binding. Once crRNA is bound, the catalytic loops and β-hairpins implicated in base

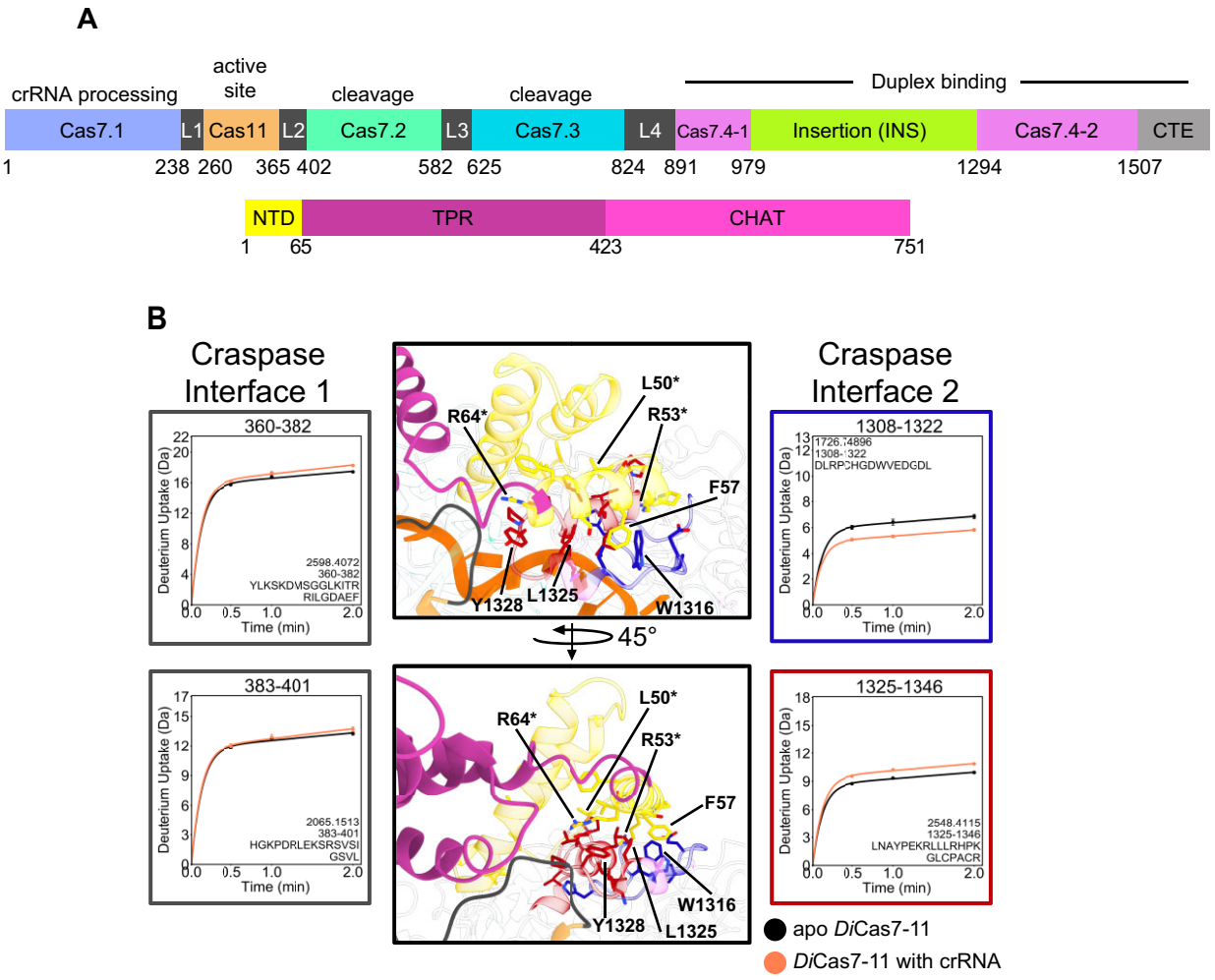

Figure 9. HDX–MS analysis of the regions of *Di*Cas7-11-crRNA responsible for TPR-CHAT binding. (**A**) Primary sequence and domains of *Di*Cas7-11 and *Di*TPR-CHAT colored by domains. (**B**) CI1 remains solvent exposed upon crRNA binding (dark gray), while a decrease in exchange in residues 1308–1322 (red) and an increase in exchange in residues 1325–1346 (blue) was observed. This suggests a conformational change within CI2. Residues in *Di*Cas7-11 and TPR-CHAT^{NTD} that form a hydrophobic interface are labeled accordingly (PDB: 7YND). Residues L50, R53, and R64 (marked by asterisks) when mutated to alanine abrogated interaction between *Di*Cas7-11 and *Di*TPR-CHAT^{NTD}.

flipping become structured. The fact that *Di*Cas7-11-crRNA$_{57}$ shows lower cleavage activity than *Di*Cas7-11-crRNA$_{37}$ is consistent with the idea that only the fully formed complex is catalytically active. Upon tgRNA binding to *Di*Cas7-11-crRNA$_{37}$, the INS conformational equilibrium shifts to the less protected state. In other words, the INS domain appears to be mostly in a state that associates less well with the 3′ end of the tgRNA and 5′ end of the crRNA in the ternary complex. The increased exposure of the INS upon tgRNA binding suggests that the INS is disengaged during target cleavage consistent with the observation of equal cleavage activity for *Di*Cas7-11(ΔINS)-crRNA versus *Di*Cas7-11-crRNA.

Large decreases in solvent exchange were observed along the crRNA-binding surface. Comparison with analysis of changes in SASA indicated these changes could only be accounted for by a disorder to order transition upon crRNA binding. The thumb-like β-hairpins that extend from Cas7.1 to Cas7.2, Cas7.2 to Cas7.3, and Cas7.3 to Cas7.4 all show dramatic decreases in exchange upon crRNA binding. These motifs sandwich the flipped base in the crRNA against the subsequent domain's α1-helix (e.g. Cas7.2 β-hairpin to Cas7.3 α1-helix) which is already more well-folded and interacts with crRNA according to our SASA analysis [18, 19, 21]. HDX–MS reveals that crRNA binding also orders the Cas7.2 and Cas7.3 catalytic loops. We sought to see whether this behavior was observed in other type III effectors, of which there are only ancestral multiprotein complexes (e.g. type III-A and type III-B). In the absence of crRNA, the thumb-like β-hairpin and catalytic loop of a Cas7-like *Methanocaldococcus jannaschii* Csm subcomplex (type III-A) was disordered and lacked electron density (PDB: 4QTS) whereas in the presence of crRNA in a cryo-EM structure of the *Thermococcus onnurineus* type III-A Cas protein, the thumb-like β-hairpin and catalytic loop are structured (PDB: 6MUU) [15, 54]. This sole example is not a very satisfying comparison considering that the apo protein was a subcomplex and the crRNA-bound structure was a full complex, and they are from different orthologs. Thus, our HDX–MS data provide the first information about any type III protein in both the apo and crRNA-bound states reflecting ordering of the thumb-like β-hairpin and catalytic loop that may be seen in other type III effectors.

The marked decrease in exchange in both Cas11 α2-helix (residues 283–295) and the helical turn of the Cas7.3 catalytic loop upon crRNA-binding, with no accompanying

SASA changes, suggests formation of a new interface between Cas11 and the Cas7.3 domain [19, 21]. This new interaction may be facilitated by a nascent hydrophobic interaction between P643 and a crRNA base at position 5. The Cas11 α2-helix residue R283 which appears to be ordered upon crRNA binding has been implicated in positioning the scissile phosphate in structural [18, 19, 21, 26] and mutagenesis studies [20, 41]. The lack of changes in deuterium uptake upon tgRNA binding throughout the Cas11 domain (Fig. 6B and Supplementary Fig. S5) is consistent with previous structural comparisons between the binary and ternary complexes that show only slight translations and rotations [21, 41] in Cas11 upon tgRNA binding, likely related to Cas11–tgRNA interaction. Thus, coordination of scissile phosphates appears to be mediated by tgRNA binding (Fig. 6, black arrows), while structuring of Cas11 is accomplished by crRNA binding.

Changes in exchange upon tgRNA binding to the Cas7-11–cRNA complex are indicative of further conformational rearrangements in the catalytic loops. A concomitant increase in solvent accessibility in residues 411–423 and decrease in solvent accessibility in residues 424–430 in Cas7.2 (Fig. 5B) suggest a rearrangement of the flexible catalytic loop. Importantly, it suggests that tgRNA binding is required for proper positioning of the catalytic residue. TgRNA binding causes a bimodal deuterium uptake distribution in the catalytic loop of Cas7.3, residues 634–657 suggesting two slowly interconverting states. The induced motion upon tgRNA binding hints that tgRNA binding promotes motions necessary for catalysis.

Finally, it is thought that crRNA binding promotes TPR-CHAT binding [21]. HDX–MS data proved to be useful in characterizing *Di*Cas7-11 motifs that lack structure prior to crRNA binding but are involved in TPR-CHAT binding [19, 21, 25, 26]. The HDX–MS results revealed a simultaneous decrease and increase in solvent accessibility within the disordered CI2 TPR-CHAT binding motif upon crRNA binding. Such HDX behavior is evidence of a conformational change that may expose residues 1325–1346 for interaction with the TPR-CHAT^{NTD} α-helix. Residues 1325–1346 form a hydrophobic interface, the largest of all *Di*Cas7-11-TPR-CHAT interfaces, with a TPR-CHAT^{NTD} α-helix containing three residues required for formation of the Craspase complex. We did not observe any differences in the *Di*Cas7-11 CI1 motif upon crRNA binding, consistent with it being less important for TPR-CHAT binding.

Our results provide a first glimpse of an apo type III-E effector, revealing that its Cas7 domains are loosely associated and the RRM insertion sequences are unstructured. When crRNA binds, Cas7 domain interactions are solidified, the β-hairpins that flip the crRNA bases, and the catalytic loops become structured. Importantly, crRNA binding remodels the CI2 loop that is critical for TPR-CHAT binding. When tgRNA binds, the β-hairpins are remodeled likely facilitating tgRNA base-flipping. The catalytic loops are remodeled, and their dynamics are altered, likely to promote catalysis. As the first RNA-targeting single-protein effector without collateral cleavage [11], biophysical characterization of *Di*Cas7-11 may prove informative for developing RNA editing tools and therapies [55, 56].

Acknowledgements

We thank Steve Silletti for assistance and mentorship in operating the mass spectrometer.

Author contributions: Calvin P. Lin (Conceptualization, Formal analysis, Investigation, Methodology, Writing—original draft), Harry Li (Investigation), Tianqi Wang (Investigation), Daniel J. Brogan (Investigation, Methodology, Writing—review & editing), Omar S. Akbari (Resources, Supervision), and Elizabeth A. Komives (Methodology, Resources, Supervision, Writing—original draft)

Supplementary data

Supplementary data is available at NAR online.

Conflict of interest

O.S.A. is a founder of Agragene Inc. and Synvect Inc. with equity interest. The terms of this arrangement have been reviewed and approved by the University of California, San Diego in accordance with its conflict of interest policies.

Funding

C.P.L. acknowledges support from the Molecular Biophysics Training Grant from the NIH T32 GM008326. This work was supported by NIH/NIAID (R01AI151004) awarded to O.S.A.

Data availability

The raw HDXMS data files and analyzed data are available at massive.ucsd.edu dataset MSV000095504. Uptake plots may be generated from the state data excel file using the DECA program available at https://github.com/komiveslab/DECA and https://zenodo.org/records/15066277.

References

1. Barrangou R, Fremaux C, Deveau H *et al.* CRISPR provides acquired resistance against viruses in prokaryotes. *Science* 2007;**315**:1709–12. https://doi.org/10.1126/science.1138140
2. Hille F, Richter H, Wong SP *et al.* The biology of CRISPR–Cas: backward and forward. *Cell* 2018;**172**:1239–59. https://doi.org/10.1016/j.cell.2017.11.032
3. Liu TY, Doudna JA. Chemistry of class 1 CRISPR–Cas effectors: binding, editing, and regulation. *J Biol Chem* 2020;**295**:14473–87.
4. Liu L, Li X, Wang J *et al.* Two distant catalytic sites are responsible for C2c2 RNase activities. *Cell* 2017;**168**:121–34.e12. https://doi.org/10.1016/j.cell.2016.12.031
5. Yan WX, Chong S, Zhang H *et al.* Cas13d is a compact RNA-targeting type VI CRISPR effector positively modulated by a WYL-domain-containing accessory protein. *Mol Cell* 2018;**70**:327–39.e5. https://doi.org/10.1016/j.molcel.2018.02.028
6. Yang H, Patel DJ. Structures, mechanisms and applications of RNA-centric CRISPR–Cas13. *Nat Chem Biol* 2024;**20**:673–88. https://doi.org/10.1038/s41589-024-01593-6
7. Kellner MJ, Koob JG, Gootenberg JS *et al.* SHERLOCK: nucleic acid detection with CRISPR nucleases. *Nat Protoc* 2019;**14**:2986–3012. https://doi.org/10.1038/s41596-019-0210-2
8. Brogan DJ, Chaverra-Rodriguez D, Lin CP *et al.* Development of a rapid and sensitive CasRx-based diagnostic assay for SARS-CoV-2. *ACS Sens* 2021;**6**:3957–66. https://doi.org/10.1021/acssensors.1c01088
9. Buchman AB, Brogan DJ, Sun R *et al.* Programmable RNA targeting using CasRx in flies. *CRISPR J* 2020;**3**:164–76. https://doi.org/10.1089/crispr.2020.0018
10. Wang Q, Liu X, Zhou J *et al.* The CRISPR–Cas13a gene-editing system induces collateral cleavage of RNA in glioma cells. *Adv Sci* 2019;**6**:1901299. https://doi.org/10.1002/advs.201901299

11. Özcan A, Krajeski R, Ioannidi E *et al.* Programmable RNA targeting with the single-protein CRISPR effector Cas7-11. *Nature* 2021;**597**:720–5. https://doi.org/10.1038/s41586-021-03886-5
12. van Beljouw SPB, Haagsma AC, Rodríguez-Molina A *et al.* The gRAMP CRISPR–Cas effector is an RNA endonuclease complexed with a caspase-like peptidase. *Science* 2021;**373**:1349–53.
13. Schmitt-Ulms C, Kayabolen A, Manero-Carranza M *et al.* Programmable RNA writing with trans-splicing. bioRxiv, https://doi.org/10.1101/2024.01.31.578223, 1 February 2024, preprint: not peer reviewed.
14. Nemudraia A, Nemudryi A, Wiedenheft B. Repair of CRISPR-guided RNA breaks enables site-specific RNA excision in human cells. *Science* 2024;**384**:808–14. https://doi.org/10.1126/science.adk5518
15. Jia N, Mo CY, Wang C *et al.* Type III-A CRISPR–Cas Csm complexes: assembly, periodic RNA cleavage, DNase activity regulation, and autoimmunity. *Mol Cell* 2019;**73**:264–77.e5. https://doi.org/10.1016/j.molcel.2018.11.007
16. Taylor DW, Zhu Y, Staals RHJ *et al.* Structural biology. Structures of the CRISPR–Cmr complex reveal mode of RNA target positioning. *Science* 2015;**348**:581–5. https://doi.org/10.1126/science.aaa4535
17. Osawa T, Inanaga H, Sato C *et al.* Crystal structure of the CRISPR–Cas RNA silencing Cmr complex bound to a target analog. *Mol Cell* 2015;**58**:418–30. https://doi.org/10.1016/j.molcel.2015.03.018
18. Kato K, Zhou W, Okazaki S *et al.* Structure and engineering of the type III-E CRISPR–Cas7-11 effector complex. *Cell* 2022;**185**:2324–37.e16. https://doi.org/10.1016/j.cell.2022.05.003
19. Goswami HN, Rai J, Das A *et al.* Molecular mechanism of active Cas7-11 in processing CRISPR RNA and interfering target RNA. *eLife* 2022;**11**:e81678. https://doi.org/10.7554/eLife.81678
20. Hu C, van Beljouw SPB, Nam KH *et al.* Craspase is a CRISPR RNA-guided, RNA-activated protease. *Science* 2022;**377**:1278–85. https://doi.org/10.1126/science.add5064
21. Huo Y, Zhao H, Dong Q *et al.* Cryo-EM structure and protease activity of the type III-E CRISPR–Cas effector. *Nat Microbiol* 2023;**8**:522–32. https://doi.org/10.1038/s41564-022-01316-4
22. Behler J, Sharma K, Reimann V *et al.* The host-encoded RNase E endonuclease as the crRNA maturation enzyme in a CRISPR–Cas subtype III-bv system. *Nat Microbiol* 2018;**3**:367–77. https://doi.org/10.1038/s41564-017-0103-5
23. Hatoum-Aslan A, Samai P, Maniv I *et al.* A ruler protein in a complex for antiviral defense determines the length of small interfering CRISPR RNAs. *J Biol Chem* 2013;**288**:27888–97. https://doi.org/10.1074/jbc.M113.499244
24. Strecker J, Demircioglu FE, Li D *et al.* RNA-activated protein cleavage with a CRISPR-associated endopeptidase. *Science* 2022;**378**:874–81. https://doi.org/10.1126/science.add7450
25. Kato K, Okazaki S, Schmitt-Ulms C *et al.* RNA-triggered protein cleavage and cell growth arrest by the type III-E CRISPR nuclease-protease. *Science* 2022;**378**:882–9. https://doi.org/10.1126/science.add7347
26. Hong T, Luo Q, Ma H *et al.* Structural basis of negative regulation of CRISPR–Cas7-11 by TPR-CHAT. *Sig Transduct Target Ther* 2024;**9**:111. https://doi.org/10.1038/s41392-024-01821-4
27. Brogan DJ, Benetta ED, Wang T *et al.* Synthetic type III-E CRISPR–Cas effectors for programmable RNA-targeting. bioRxiv, https://doi.org/10.1101/2024.02.23.581838, 24 February 2024, preprint: not peer reviewed.
28. Malakhov MP, Mattern MR, Malakhova OA *et al.* SUMO fusions and SUMO-specific protease for efficient expression and purification of proteins. *J Struct Func Genom* 2004;**5**:75–86. https://doi.org/10.1023/B:JSFG.0000029237.70316.52
29. Lumpkin RJ, Ahmad AS, Blake R *et al.* The mechanism of NEDD8 activation of CUL5 ubiquitin E3 ligases. *Mol Cell Proteomics* 2021;**20**:100019. https://doi.org/10.1074/mcp.RA120.002414
30. Lumpkin RJ, Komives EA. DECA, A comprehensive, automatic post-processing program for HDX–MS data. *Mol Cell Proteomics* 2019;**18**:2516–23. https://doi.org/10.1074/mcp.TIR119.001731
31. Masson GR, Burke JE, Ahn NG *et al.* Recommendations for performing, interpreting and reporting hydrogen deuterium exchange mass spectrometry (HDX–MS) experiments. *Nat Methods* 2019;**16**:595–602. https://doi.org/10.1038/s41592-019-0459-y
32. Makarova KS, Wolf YI, Iranzo J *et al.* Evolutionary classification of CRISPR–Cas systems: a burst of class 2 and derived variants. *Nat Rev Micro* 2020;**18**:67–83. https://doi.org/10.1038/s41579-019-0299-x
33. Komives EA. Dynamic allostery in thrombin—a review. *Front Mol Biosci* 2023;**10**:1200465. https://doi.org/10.3389/fmolb.2023.1200465
34. Truhlar S, Torpey J, Komives E. Regions of IkappaBalpha that are critical for its inhibition of NF-kappaB.DNA interaction fold upon binding to NF-kappaB. *Proc Natl Acad Sci USA* 2006;**103**:18951–6. https://doi.org/10.1073/pnas.0605794103
35. Truhlar S, Croy C, Torpey J *et al.* Solvent accessibility of protein surfaces by amide H/2H exchange MALDI-TOF mass spectrometry. *J Am Soc Mass Spectrom* 2006;**17**:1490–7. https://doi.org/10.1016/j.jasms.2006.07.023
36. Kolesnik MV, Fedorova I, Karneyeva KA *et al.* Type III CRISPR–Cas systems: deciphering the most complex prokaryotic immune system. *Biochemistry Moscow* 2021;**86**:1301–14. https://doi.org/10.1134/S0006297921100114
37. Benda C, Ebert J, Scheltema RA *et al.* Structural model of a CRISPR RNA-silencing complex reveals the RNA-target cleavage activity in Cmr4. *Mol Cell* 2014;**56**:43–54. https://doi.org/10.1016/j.molcel.2014.09.002
38. Konermann L, Tong X, Pan Y. Protein structure and dynamics studied by mass spectrometry: H/D exchange, hydroxyl radical labeling, and related approaches. *J Mass Spectrom* 2008;**43**:1021–36. https://doi.org/10.1002/jms.1435
39. James EI, Murphree TA, Vorauer C *et al.* Advances in hydrogen/deuterium exchange mass spectrometry and the pursuit of challenging biological systems. *Chem Rev* 2022;**122**:7562–623. https://doi.org/10.1021/acs.chemrev.1c00279
40. Torres-Paris C, Song HJ, Engelberger F *et al.* The light chain allosterically enhances the protease activity of Murine urokinase-type plasminogen activator. *Biochemistry* 2024;**63**:1434–44. https://doi.org/10.1021/acs.biochem.4c00071
41. Yu G, Wang X, Zhang Y *et al.* Structure and function of a bacterial type III-E CRISPR–Cas7-11 complex. *Nat Microbiol* 2022;**7**:2078–88. https://doi.org/10.1038/s41564-022-01256-z
42. Liu X, Zhang L, Wang H *et al.* Target RNA activates the protease activity of Craspase to confer antiviral defense. *Mol Cell* 2022;**82**:4503–18.e8. https://doi.org/10.1016/j.molcel.2022.10.007
43. Nishimasu H, Nureki O. Structures and mechanisms of CRISPR RNA-guided effector nucleases. *Curr Opin Struct Biol* 2017;**43**:68–78. https://doi.org/10.1016/j.sbi.2016.11.013
44. Ekundayo B, Torre D, Beckert B *et al.* Structural insights into the regulation of Cas7-11 by TPR-CHAT. *Nat Struct Mol Biol* 2023;**30**:135–9. https://doi.org/10.1038/s41594-022-00894-5
45. Deltcheva E, Chylinski K, Sharma CM *et al.* CRISPR RNA maturation by trans-encoded small RNA and host factor RNase III. *Nature* 2011;**471**:602–7. https://doi.org/10.1038/nature09886
46. Stella G, Marraffini L. Type III CRISPR–Cas: beyond the Cas10 effector complex. *Trends Biochem Sci* 2024;**49**:28–37. https://doi.org/10.1016/j.tibs.2023.10.006
47. Burgess DJ. New cuts for CRISPR effectors. *Nat Rev Genet* 2023;**24**:71. https://doi.org/10.1038/s41576-022-00570-w
48. Engen JR, Komives EA. Complementarity of hydrogen/deuterium exchange mass spectrometry and cryo-electron microscopy. *Trends Biochem Sci* 2020;**45**:906–18. https://doi.org/10.1016/j.tibs.2020.05.005

49. Cui N, Zhang J-T, Li Z *et al.* Structural basis for the non-self RNA-activated protease activity of the type III-E CRISPR nuclease-protease Craspase. *Nat Commun* 2022;**13**:7549. https://doi.org/10.1038/s41467-022-35275-5
50. Maris C, Dominguez C, Allain F. The RNA recognition motif, a plastic RNA-binding platform to regulate post-transcriptional gene expression. *FEBS J* 2005;**272**:2118–31. https://doi.org/10.1111/j.1742-4658.2005.04653.x
51. Nagai K, Oubridge C, Jessen T *et al.* Crystal structure of the RNA-binding domain of the U1 small nuclear ribonucleoprotein A. *Nature* 1990;**348**:515–20. https://doi.org/10.1038/348515a0
52. Oubridge C, Ito N, Evans P *et al.* Crystal structure at 1.92A resolution of the RNA-binding domain of the U1A spliceosomal protein complexed with an RNA hairpin. *Nature* 1994;**372**:432–8. https://doi.org/10.1038/372432a0
53. Wang S, Guo M, Zhu Y *et al.* Cryo-EM structure of the type III-E CRISPR–Cas effector gRAMP in complex with TPR-CHAT. *Cell Res* 2022;**32**:1128–31. https://doi.org/10.1038/s41422-022-00738-3
54. Numata T, Inanaga H, Sato C *et al.* Crystal structure of the Csm3–Csm4 subcomplex in the type III-A CRISPR–Cas interference complex. *J Mol Biol* 2015;**427**:259–73. https://doi.org/10.1016/j.jmb.2014.09.029
55. Koonin EV, Gootenberg JS, Abudayyeh OO. Discovery of diverse CRISPR–Cas systems and expansion of the genome engineering toolbox. *Biochemistry* 2023;**62**:3465–87. https://doi.org/10.1021/acs.biochem.3c00159
56. Catchpole RJ, Terns MP. New type III CRISPR variant and programmable RNA targeting tool: oh, thank heaven for Cas7-11. *Mol Cell* 2021;**81**:4354–6. https://doi.org/10.1016/j.molcel.2021.10.014

Received: September 13, 2024. **Revised:** March 19, 2025. **Editorial Decision:** March 20, 2025. **Accepted:** March 30, 2025